Distribution of organic matter and diatom frustules (diversity, flux) along the western Indian continental shelf related to contrasting physicochemical settings

Medhavi Pandey[1, 2#], Haimanti Biswas[1, 2*$] and Sabine Schmidt[3@]

[1]CSIR National Institute of Oceanography, Biological Oceanography Division, Dona Paula, Goa-403004, India.

[2]Academy of Scientific and Innovative Research (AcSIR), Ghaziabad-201002, India

[3]Université de Bordeaux, CNRS Bordeaux INP, EPOC, UMR 5805, F-33600 Pessac, France

[*]Corresponding author: haimanti.biswas@nio.res.in; haimanti.biswas.nio@gmail.com

[#]ORCID ID https://orcid.org/0000-0001-8243-3229

[$]ORCID ID https://orcid.org/0000-0003-1869-1308

[@]ORCID ID https://orcid.org/0000-0002-5985-9747

Abstract

The western Indian continental shelf (eastern Arabian Sea) exhibits contrasting biogeochemical features. This area becomes highly productive due to summer monsoon-driven coastal upwelling in the south and winter monsoon-induced convective mixing in the north. Additionally, in the northern self, the eastern boundary of the Oxygen Minimum Zone (OMZ) persists but is absent in the south. Phytoplankton blooms are dominated by diatoms that contribute to sedimentary phytodetritus flux supplying major elements (C, N, Si) and food for benthic biota and hence important to address. Here we present the data on organic matter content, diatom frustule flux, abundance, and diversity using surface sediments (core tops collected using a multicorer) from 6 locations (11–21° N) along the shelf in a 2° interval at 200 m isobaths. The organic matter retrieved from the core top was relatively fresh (nearly ~4.5 years old) as evident from ^{210}Pb profiles Frustule abundance and diversity (the maximum at 15° N and minimum at 19° N) varied from 0.10–18.46 $\times 10^4$ valves g^{-1} and 0.79–2.32, respectively. A total of 36 diatom genera were found with two centric (*Thalassiosira* and *Coscinodiscus*), and one pennate (*Nitzschia*) diatoms as major contributors. The higher contribution of *Thalassiosira* was observed throughout the shelf dominating the south (11, 13, 15° N), whereas, in the north (17, 19, 21° N) *Coscinodiscus* was dominant. The highest organic matter content (3.4%) and frustule abundance (18.46×10^4 valves g^{-1}) were seen at 15° N despite low diatom valve flux (3.3×10^3 valves cm^{-2} yr^{-1}) and could be due to the influence of OMZ, where organic matter is well preserved. Contrarily, the upwelling-influenced station in the south (at 11° N) exhibited the highest diatom valve flux (10.14×10^3 valves cm^{-2} yr^{-1}) however low organic matter content (1.6 %) and frustule abundance (4.99×10^4 valves g^{-1}) was attributed to faster mineralization. This study suggested that the preservation potential of organic matter varies across the shelf and is likely to control its recycling, impacting nutrient release and resources for the benthic community.

Keywords: Eastern Arabian Sea; Continental shelf; Phytoplankton; Diatom frustules; Particulate organic matter export

1. Introduction

Continental shelves are responsible for storing ~45% of organic carbon in the underlying sediments (Hedges and Keil, 1995). Most of the organic matter produced by marine phytoplankton is recycled in the upper water column (100 m), with a fraction sinking into the sediment (Volk and Hoffert, 1985). The sinking of phytodetritus is controlled by several factors, including the rates of primary production, phytoplankton community composition, remineralization, sinking velocity, cell size, zooplankton abundance and grazing, dissolved oxygen concentration, temperature, etc. (Banse, 1990; De La Rocha et al., 2008; Le Moigne et al., 2015; Cavan et al., 2015; Le Moigne et al., 2016). After reaching the sediment, a substantial portion of the organic matter can be recycled. A high organic matter remineralization rate of ~80–90% of the spring bloom was reported from the Californian upwelling system (Falkowski et al., 1988). A small proportion (1–4%) of the initial bloom is preserved in the sediments (Abrantes et al., 2002). The preservation/loss of organic matter in the sediment is controlled by several physical, chemical, and biological factors such as sediment texture, availability of dissolved oxygen, temperature, benthic biota, microbial degradation, sedimentation intensity, etc. (Keil et al., 2016 and references therein). Among all, insufficient dissolved oxygen can potentially slow down microbial degradation and reduce the presence of grazers. Dissolved oxygen level is therefore a criticall parameter in remineralization of sedimentary phytodetritus (Keil et al., 2016).

The Arabian Sea, a part of the north Indian Ocean, is a semi-enclosed tropical basin that exhibits high spatial variability in physical forcing and biogeochemical features (Figure 1). This region shows one of the highest primary productivity rates among other oceanic regions in the world (Sawant and Madhupratap, 1996). The Arabian Sea is also a place where the thickest oxygen minimum zone (OMZ) (<0.5 mL L^{-1}) is present within 200 - 1200 m towards the eastern side. This OMZ is mostly governed by high productivity and limited ventilation of the subsurface waters (Naqvi et al., 1994; Liu et al., 2024). The eastern boundary of the OMZ lies within a major area of the Western Indian continental shelf (Fig. 1A), extending slightly above 14° N and 25° N. In a study in the Arabian Sea, it was noticed that the OMZ was associated with slower organic matter mineralization, facilitating higher preservation in the sediment (Keil et al., 2016). Likewise, our previous study from the northcentral Arabian Sea showed that the hotspots for organic matter preservation were within the core OMZ (Pandey et al., 2023).

The reversing monsoon winds are the major forcing in the Eastern Arabian Sea (Western Indian Continental Shelf), making it a productive coastal province with high variability (seasonally and spatially) (Prasanna Kumar et al., 2000), which is usually not found elsewhere (Shetye et al., 1994). The major boundary current system present in the eastern Arabian Sea is the West India Coastal Current (WICC) (Shankar and Shetye, 1997) that flows equatorward during the summer months (April onwards) and reverses with the onset of winter (November) (Figs. 1A-B). This entire shelf region exhibits contrasting features from south to north in terms of physical properties (salinity, temperature) as well as biogeochemistry during both summer (Silori et al., 2021; Chowdhury and Biswas, 2023) and winter monsoons (Vijayan et al., 2021; Albin et al., 2022). Usually, the northern shelf is characterized by the presence of high sea surface salinity (>36 PSU), in contrast to the southern part of the shelf where low salinity (<34 PSU) waters prevail due to more freshwater discharge (summer monsoon) and the influence of Bay of Bengal low saline waters (winter monsoon).

During the summer monsoon (June-September), the southwesterly wind blows over the Arabian Sea and the alongshore components of this wind generate weak to moderate upwelling along the southwestern part of the shelf (Shetye et al., 1990) (Fig. 1A). The upwelling-induced nutrient enrichment and subsequent phytoplankton bloom is usually observed between 8 -15° N (Habeebrehman et al., 2008 and references therein). The coastal areas north of 15 °N remain relatively low in productivity compared to the south (Albin et al., 2022; Chowdhury and Biswas, 2023) because the upwelled waters propagate further northward but mostly remain below 30 m depth and were not seen to reach the surface (Shah et al., 2015). During the winter monsoon (Nov-Feb), the cold and dry northeasterly wind blows from the Himalayan region (Tibetian plateau) towards the Arabian Sea, leading to evaporative cooling of surface waters with subsequent convective mixing in the northern Arabian Sea (Banse and McClain, 1986; Madhupratap et al., 1996) (Fig. 1B). Cold nutrient-rich subsurface waters are upwelled to the surface, where they support the development of high phytoplankton biomass (Banse and McClain, 1986; Madhupratap et al., 1996). Thus, in the eastern Arabian Sea, the monsoon winds are the key drivers of natural nutrient enrichment events, which in turn support large diatom-dominated phytoplankton blooms (e.g. *Coscinodiscus*, *Rhizosolenia*, *Chaetoceros*, and *Fragilaria*) and associated fisheries (Nair and Subrahmanyan, 1955; Subrahmanyan, 1959; Sawant and Madhupratap, 1996; Habeebrehman et al., 2008; Vijayan et al., 2021).

For the vertical transfer of particles, diatoms are of high geochemical importance as they transport particulate silica, carbon, and nitrogen rapidly to great depths (Scharek et al., 1999). Due to their ballasted silica shell (frustules), these microscopic biosilicifiers can facilitate a substantial export of fast-sinking phytodetrital aggregates to the seabed (Lampitt, 1985). Earlier studies from major upwelling systems (Benguela, Iberia-Canary, California, Peru-Humboldt, and Oman-Somali) indicated a positive correlation between diatom frustule abundance and organic carbon in sediments, suggesting that sedimentary diatoms (number of valves g^{-1}) as representative of carbon export (Schuette and Schrader, 1981; Abrantes, 1988; Abrantes et al., 2016). In a sediment trap study from the Scotia Sea (Southern Ocean), it was observed that diatoms play a key role in exporting carbon and silicon to the deeper depths (Zúñiga et al. 2021).

In the coastal and offshore Arabian Sea, diatoms contribute nearly 86% to the total phytoplankton standing stock mostly during productive periods like the summer and winter monsoons (Subramanyam and Sarma, 1965; Gauns et al., 2005; Chowdhury et al., 2021; Chowdhury and Biswas, 2023). Hence, it is expected that diatoms can contribute significantly to the transport of organic matter to the sediment after the diatom bloom had ended. However, there may be a seasonal shift in the diatom-dominated phytodetrital flux as the northern shelf becomes nutrient -poor during the summer and the southern shelf during the winter monsoons dominated by smaller phytoplankton (Vijayan et al., 2021; Silori et al., 2022; Albin et al., 2022). The diatom-derived phytodetritus deposited on the surface sediment usually represents the organic matter accumulated throughout the year and can be considered to study its diversity, flux, and preservation in relation to the prevailing biogeochemical conditions in the sediment as well as in the overlying water column. Likewise, our previous studies (Pandey et al. 2023; 2024) on the surface sediments of the central Arabian Sea showed high abundances of diatom frustules correlated with organic matter content. Surface ocean processes driven by atmospheric forcing and the presence of the OMZ were found to be the key factors responsible for the observed spatial variability. However, not all diatoms can efficiently export carbon to the sediment and it depends on their frustule thickness, size, and morphology (chain formation) (Abrantees et al. 2002; Pandey et al 2023; 2024). The thickly silicified large

diatoms like *Coscinodiscus* and *Rhizosolenia* may also escape grazing and sink faster (Pandey et al. 2023; 2024). On the other hand, small chain-forming diatoms like *Thalassiosira* may sink efficiently due to ballast. Thinly silicified cells like *Chaetoceros* or *Leptocylindrus* may not make their way to the sediment as their frustules can be either grazed or fragmented and easily dissolved even after reaching the sediment. Thus, analyzing the diversity of diatom frustules is crucial to understanding their potential to export carbon to the sediment. However, such information is missing for the West Indian continental shelf.

To fill this lacuna, this study investigates for the first time the distribution and preservation of organic matter and diatom frustules along the western Indian continental shelf, emphasising their relationships with the unique biogeochemical settings of this region. This study further addresses key questions about the sources, degradation processes, and preservation of diatom frustules and organic matter under varying physicochemical conditions along the shelf. Such information may be useful to improve our understanding of the role of diatom frustules in exporting organic matter to the shelf sediment and related biogeochemistry. Particularly, the north-south spatial variability of the OMZ along the shelf may also be an important factor governing the preservation/loss of organic matter and frustules in the sediment. Using the literature, we also attempted to relate the diversity of diatom frustules from the water column with the observed variability in their flux and abundance from the sediment.

2. Materials and methods

2.1 Sample collection

The sediment sampling was done onboard *R.V. Sindhu Sadhana* (SSD-068) from the Eastern Arabian Sea from December 2019 to January 2020 (Figs. 1–2). Short well-preserved interface cores were collected from 6 different locations (21°, 19°, 17°, 15°, 13°, and 11° N) along 200 m isobath using a multi-corer (Ocean Scientific International Limited Maxi, UK). The cores were subsampled immediately after collection, extrudeded vertically at 0.5 cm interval, kept in clean vials with screw caps, and stored in the dark at 4°C until further analyses. The surface layer (0–0.5 cm) of the undisturbed sediment core has been used for the present study. The samples were later processed in the laboratory and analyzed for sedimentation rate, total carbon (TC), total inorganic carbon (TIC), total nitrogen (TN), and diatom frustules. Dry bulk density (DBD) was determined by measuring the sediment weight before and after drying at 62°C and assuming a sediment density of 2.65 g cm^{-3}.

2.2 Analytical method

2.2.1 Core dating

The mass accumulation rates (MAR; g cm^{-2} yr^{-1}) of four sites (11, 13, 15, and 17° N) were determined using ^{210}Pb (T1/2 = 22.3 years), a naturally occurring radionuclide. ^{210}Pb from atmospheric fallout and water column production is readily scavenged on suspended sediment (Schmidt et al., 2014). Once deposited on the seafloor, ^{210}Pb in excess ($^{210}Pb_{xs}$) then decreases with depth in the sediment according to its half-life and sedimentation intensity. The radionuclides of interest (^{210}Pb, ^{226}Ra) were measured in sediment sampled using a high-efficiency, low-background well-type gamma detector equipped with a Cryocycle at EPOC (University of Bordeaux, France). Calibration of the detector was achieved using certified reference material (IAEA-RGU-1). The excesses of ^{210}Pb, expressed in mBq g^{-1}, were calculated as the difference between the measured total activity of ^{210}Pb and that of its parent isotope (^{226}Ra). Sediment and mass accumulation rates were calculated from the $^{210}Pb_{xs}$ profile versus

sediment depth or cumulative mass based on the constant flux constant sediment (CF:CS) model (Schmidt et al, 2014).

MARs for the samples from 19–21° N were not determined due to technical problems. From the available literature (Somayajulu et al., 1999), we have used the 21° N sedimentation rate in a location and water depth (280 m) close to our sampling site (water depth of 200 m). We could not find any suitable data for 19° N to compare.

2.2.2 Total inorganic carbon (TIC), total organic carbon (TOC), and total nitrogen (TN) contents

Aliquots of sediment samples were oven-dried (at 60°C overnight), ground in an agate mortar and pestle, and kept in vials for further analysis. For determining the total carbon (TC) and total nitrogen (TN), a 10 mg homogenized sediment sample was placed in tin capsules and measured using a CHN Elemental analyzer (Euro Vector EA3000 series analyzer, Central Analytical Facility, CSIR-NIO, Goa, India) against a soil reference material NC (Thermo Fisher Scientific, Cambridge, UK) with an analytical error of <2%. Total inorganic carbon (TIC) was measured using a coulometer with an acidification module (Model CM5015) against the calcium carbonate ($CaCO_3$) standard (Merck, Germany). The accuracy and precision of the results were found to vary by ±1.25%. The CaCO3 % is calculated using TIC% × 8.33. The difference between the TC and TIC contents yielded the total organic carbon (TOC) content [TOC=TC-TIC].

2.2.3 Analysis of diatom frustules

The dried sediments were treated as suggested by Armbrecht et al. (2018) to remove carbonates, organic matter and clay minerals present in the sediments. Small portions of the oven-dried samples (50 mg) were taken in clean polypropylene tubes (50 mL) and first treated with 5 mL of HCl (10%) and kept aside for 4–5 hours letting to dissolve any calcareous materials (inorganic carbon) present in the sediment. Then 20 mL of Milli-Q water was added to each tube and after 24 hours, the supernatant was discarded and 25 mL of Milli-Q water was added and left again overnight. This process was repeated twice followed by the addition of 3–5 mL of H_2O_2 solution (30%) and left in the water bath at 60 °C for nearly 1 hour. After 3–4 hours, 20 mL of Milli-Q water was added and thoroughly rinsed three times by decanting the supernatant. To this sample, 10 mL of 0.01 N anhydrous sodium diphosphate ($Na_4P_2O_7$) solution was added and left undisturbed to allow fine clay particles to be suspended in the solution. These samples were then washed three more times with 20 mL of Milli-Q water. Finally, the tubes were filled with 10 mL of Milli-Q water and gently mixed. Centrifugation was avoided during this process, to avoid breakage of the frustules (Koizumi, 1985).

For enumeration and absolute abundance counting, 1 mL of the processed solution was taken and analyzed in a Sedgewick rafter counting chamber (1000 squares) (Pyser, UK) under an inverted microscope (Nikon Ti2) at 400–600× magnification. The whole slide was counted for better reproducibility of the results, and an average of 250 diatom valves were counted and identified up to the genus level. Fragments larger than half the size were considered as a whole (Abrantes and Sancetta, 1985). The following formula was used to derive the absolute abundance of diatom frustules, expressed as valves per gram of dry sediment:

$$\text{Diatom frustule (valves g}^{-1}) = \frac{Number\ of\ valves \times Volume\ \ of\ processed\ sample\ (mL)}{Sediment\ content\ (g)}$$

Based on their absolute abundance, the relative abundance (RA %) was calculated as below:

188 RA (%)= $\frac{Number\ of\ valves\ of\ individual\ diatoms \times 100}{Sum\ of\ the\ total\ diatom\ valves}$

189 Based on their RA (%), diatoms were classified as “major” (>10%) or “minor” (<10%) contributors to the total
190 assemblages. y

191 An aliquot of the processed samples was taken in a plastic petri plate and allowed to air dry overnight at
192 room temperature and the dry samples were examined for photography using a scanning electron microscope
193 (SEM) model JEOL-JSM IT300 (JEOL Ltd., Tokyo, Japan) available at the central analytical facility at the CSIR-
194 National Institute of Oceanography, Goa. Prior to SEM analysis dry samples were mounted on a SEM stub and
195 sputtered with gold. Photographs of some selected diatoms were taken at a variable magnification (1,000–5,000×).

196 Identification of diatom genera was mostly done using identification keys from Desikachary (1989), Tomas
197 (1997), and in some cases species-specific monographs (The Academy of Natural Science, Drexel University
198 (ANSP diatoms; http://symbiont.ansp.org/dntf/gallery.php?g=Nitzschia&r=G-L). For some genera, the initial
199 information was also fetched from https://www.algaebase.org and https://www.marinespecies.org. The size of the
200 valves was measured on a pre-calibrated microscale using NIS Elements image software provided by Nikon
201 (Nikon Technologies, Japan).

202 The Shannon-Wiener Index (H′) (Shannon and Weaver, 1963) was calculated using the following formula to
203 indicate the diversity of the community that is contributed by different species in a community

204 $H' = -\sum_{i=1}^{S} pi\ ln\ ln\ (pi)$

205 where $p_i = n_i/N$ (n_i is the number of individuals of the i^{th} species in the community, and N is the total number of
206 species.

207

208 The diatom valve flux (valves $cm^{-2}\ yr^{-1}$) was calculated (Table 1) using the following formula (Kuwae et al.,
209 2006)

210 Diatom valve flux = DVC × MAR

211 or

212 Diatom valve flux = DVC × SAR × DBD

213 Where

214 DVC = Diatom Valve Concentration (valves g^{-1} of dry sediment)

215 MAR =Mass Accumulation Rate (g $cm^{-2}\ yr^{-1}$), SAR is the sedimentation rate (cm yr^{-1})

216 DBD =Dry Bulk Density (g cm^{-3})

217 **2.2.4 Statistical Analysis**

218 The relationships between biotic factors (diversity and absolute abundance of total diatom frustules,
219 centric and pennate diatoms, three major contributing genera (> 10%), and four minor diatoms contributing >3%
220 to the assemblage) and environmental variables (TC, TOC, TIC, TN) were studied using the CANOCO version

4.5 software (TerBraak and Šmilauer, 2002). Redundancy analysis (RDA), a linear multivariate model was utilized to explain the association between environmental and biological variables. It should be noted that RDA was preferred to similar statistical models such as CCA/PCA as it is more robust in explaining the relationship between the environmental factors and species variables.

3. Results

3.1 Diatom frustule flux, abundance, composition, and distribution

Based on the mass accumulation rates (MAR) from four locations (Table 1), the ages of the core tops were estimated to be 2, 3, 8.2, and 2.3 years for 11° N, 13 ° N, 15 ° N and 21° N, respectively. The age of the core top at 17° N was the highest corresponding to 30 years. The cores for the present study were collected at the end of 2019, suggesting that the phytodetritus was most likely to be generated not before 2016-2017 except at 17 ° N. The highest MAR (0.203 g cm^{-2} yr^{-1}) was observed at 11° N, whereas substantially lower values were found at the other four locations (0.093, 0.018, 0.011, and 0.096 g cm^{-2} yr^{-1} at 13, 15, 17, and 21° N, respectively). Based on MAR, the diatom valve flux was found to be as high as 10.14×10^3 valves cm^{-2} yr^{-1} at 11° N which is four times higher than the other three stations ($2.05–3.39\times10^3$ valves cm^{-2} yr^{-1}) excluding the values from 17 ° N (Table 1).

High spatial variability in diatom frustule abundance (Fig. 1C, Table 2) was documented, ranging from 0.10 to 18.46 $\times10^4$ valves g^{-1}. The highest frustule abundance was observed at 15° N (18.46 $\times10^4$ valves g^{-1}), followed by 11° N (4.99×10^4 valves g^{-1}), and the values decreased significantly at 19° N (0.10 $\times10^4$ valves g^{-1}). The average diversity index (Shannon-Wiener, H′) (Fig. 1D, Table 2) was 1.7±0.5, with the highest value (2.3) recorded at 15° N while the lowest (0.8) was documented at 19° N. Microscopic analysis revealed a total of 36 genera, including 15 centric, and 21 pennate diatoms (Fig. 2, Table 3). However, the absolute abundance of centric diatom frustule was four times higher than that of pennate diatoms, except at 15° N, where the ratio between centric and pennate diatoms was 0.6 (Supplementary Fig. 1A). Some microphotographs of major and minor contributing diatom genera are presented in Figs. 3–5.

Based on cell size, diatom frustules were classified as small (<30 μ m), medium (30–60 μm), and large (>60 μm) (Supplementary Fig. 1B). The small and medium frustules comprised the major portion of the assemblages, accounting for 39% and 53% respectively, while large frustules accounted for only 8% on average. Among the major contributing diatom genera, the size class for *Thalassiosira* and *Coscinodiscus* is presented here. An overall pattern depicted that in the case of *Thalassiosira*, the largest size fraction was the least abundant, whereas for *Coscinodiscus* it was the smallest size class (Table 4, Supplementary Fig. 1C-1D). The small and medium frustules of *Thalassiosira* (Supplementary Figs. 1C) were abundant with the highest value at 15° N (1.33×10^4 valves g^{-1} for small and 2.45×10^4 valves g^{-1}) and 11° N (0.54×10^4 valves g^{-1} for small and 2.48×10^4 valves g^{-1} for medium). The large frustules of *Coscinodiscus* were present in all stations except at 19º N. At 15º N, their absolute abundance was comparatively higher (1.35×10^4 valves g^{-1}) among other stations (Supplementary Fig. 1D). The medium frustules of *Coscinodiscus* were found in all locations. The absolute abundance of medium-sized *Coscinodiscus* frustules at 15 and 11° N was 0.18×10^4 valves g^{-1} and 0.15×10^4 valves g^{-1}, respectively (Table 4).

3.1.1 Major diatom genera

In the shelf sediment, the major diatom genera (>10% of total RA: see the method section), accounting for nearly 72.6% of the total assemblage (Supplementary Fig. 1E, Table 3), consisted of two centric [*Thalassiosira*

(Cleve) Hasle (36%) (Figs. 3A-3C, 4A) followed by *Coscinodiscus* Ehrenberg (25%)] (Figs. 3D-3E, 4B), and one pennate [*Nitzschia* Hassall (11%)] (Figs. 3F-3G, 4C). The absolute abundance of *Thalassiosira* frustule ranged from 0.03 to 4.12 $\times 10^4$ valves g^{-1} with a mean of 1.53 $\times 10^4$ valves g^{-1} (Table 3). The relative abundance of this genus ranged from 22.3 to 61.5% of the total population, with the highest value at 11° N and the lowest at 21° N (Fig. 2, Table 3). The second most abundant taxon was *Coscinodiscus* with an average absolute abundance of 0.56 $\times 10^4$ valves g^{-1} and its relative abundance ranged from 6.8 to 60.0 % with the highest and lowest values at 19° N and 11° N respectively. The chain-forming pennate diatom *Nitzschia* (average absolute abundance 0.90 $\times 10^4$ valves g^{-1}), was the third most abundant taxa with a relative abundance ranging between 3.6 and 25.0%, the highest at 15° N and the lowest at 11° N (Table 3).

3.1.2 Minor diatom genera

In general, when considering the average relative abundance of the minor contributing diatom genera (<10% of total RA) (Supplementary Fig. 1E, Table 3) (making up 27.4% of the total assemblage), the following distribution pattern was observed in descending order: *Cyclotella* (Figs. 4D, 5A)>*Thalassionema* (Fig. 4E-4F)>*Pseudo-nitzschia* (Fig. 4G, 5B)> *Fragilariopsis* (Figs. 4H, 5C-5D) >*Navicula* (Fig. 5E). The resting spores of *Chaetoceros* (Figs. 5F-5G) and *Cerataulina* (Figs. 5H-5I) were mainly found in the sediments of the stations under the influence of upwelling (11–15° N) and their relative abundance was 0.5% (Table 3). The highest number of resting spores was found at 15° N for *Chaetoceros* (900±141 g^{-1}) and at 11–13° N for *Cerataulina* (400±0 g^{-1}). Similarly, the frustules of *Fragilariopsis* (0.5–10.6%) and *Fragilaria* (0–4.2%) were documented in stations located in the south (11–15° N) and were mostly absent in the north (17–21° N) (Table 3). Genera like *Thalassionema* (3.9%), *Pseudo-nitzschia* (3.7%), and *Navicula* (1.8%) were found in most locations except at 19 °N with mean absolute frustule abundances of 0.23×10^4 valves g^{-1}, 0.28×10^4 valves g^{-1}, and 0.13×10^4 valves g^{-1}, respectively. *Cyclotella* (Fig. 5A) was observed at 11–13° N (average absolute abundance 0.19 $\times 10^4$ valves g^{-1}, corresponding to an average relative abundance of 4.5%) with a maximum relative abundance at 13° N (16.4%). Among other taxa, (Fig. 5; Table 3) *Rhizosolenia* Brightwell, *Hemidiscus* Wallich, *Diploneis* (Ehrenberg) Cleve, *Leptocylindrus* (Cleve) Petersen, *Surirella* Turpin, *Actinoptychus* Ehrenberg, etc were also present in rather low amounts. Few diatoms were found only at the selected locations, for example, *Bacillaria* at 11 and 15° N, *Synedra* at 15° N, and *Paralia* exclusively at 11° N. *Rhizosolenia* and *Hemidiscus* were observed in small fractions (average relative abundance 1.2% and 0.7%, respectively) in all locations except at 19° N. The highest relative abundance of *Diploneis* (6.7%) and *Surirella* (5.4%) was observed at station 21° N. The most diverse diatom assemblage was observed at 15° N characterized by *Nitzschia* (25%), *Thalassiosira* (22.3), *Coscinodiscus* (8.3) along with other minor contributors such as *Triceratium*, *Gomphonema*, *Odontella*, *Asterionellopsis*, *Chaetoceros*, *Pleurosigma*, *Cymbella*, *Licmophora*, *Bacteriastrum*, *Cocconeis*, *Asteromphalus*, etc (Figs. 5J-5S, Table 3).

3.2 Sedimentary inorganic and organic carbon and total nitrogen content

The TIC (%) content (Fig. 6A, Table 2) showed an average value of 7.1% with an increasing trend towards the north, except at 21° N. It varied between 2.37% and 10%, with higher values at 19° N (10%) and lower at 21° N (2.4 %). The TOC (%) content (Fig. 6B. Table 2) was almost4 times lower than the TIC, with an average value of ~2% for the entire shelf. It was the highest at 15° N (3.39 %) followed by 21° N (1.89 %) and the lowest at 19° N (0.96 %) (Fig. 6B). The highest value of $CaCO_3$ (83.6%) (Table 2) was observed at 19 ° N

and the lowest value (19.74%) was noticed at 21 °N. The TN (%) showed a similar trend to TOC along the shelf. The highest value (0.31 %) was observed at 15° N (Fig. 6C, Table 2), followed by 21° N (0.21 %) with a minimum value at 19° N (0.03%) (average 0.16 %). Both TOC and TN contents revealed significant correlations with each other (R^2= 0.93) as well as with diatom frustules (valves g^{-1} dry sediment) (R^2 = 0.88) (Figure not shown).

3.3 Statistical analysis

The RDA analysis (Fig. 7) revealed 95.8% of the relationship between the abiotic parameters (TC, TIC, TOC, TN) and the biotic components (absolute abundance of diatoms frustules, centric, pennates, individual genus, and diversity) from the first two axes. Almost 83.5% of the total variance was explained by axis 1 where TOC and TN were associated with absolute abundance (valves g^{-1}), and diversity of frustules. The abundance of the major contributing genera *Coscinodiscus*, *Thalassiosira*, and *Nitzschia* were also associated with TOC and TN on axis 1. TIC, TC, and TOC: TN were on axis 2 indicating an inverse relationship between TOC and absolute diatom abundance.

4. Discussion

Phytoplankton detritus found on the surface sediment usually represents the signature of phytoplankton biomass sinking to the seafloor throughout the year. The ^{210}Pb analysis revealed that the average age of the surface sediment was nearly 4.5 years except at 17 °N where the sediment was much older compared to the rest of the stations. A previous study by Somayajulu et al. (1999) at 21 °N (280 m depth) reported a comparable sedimentation rate corresponding to an age of 4.5 years for the surface sediment was reported. The sources of the organic matter along this productive shelf region were not addressed in the previous studies. Our earlier (2017-2018) studies from the water column in similar locations (around 200 m isobaths) using stable isotopes of particulate organic carbon ($\delta^{13}C_{POC}$) revealed an autochthonous nature of the organic matter produced by marine phytoplankton (Silori et al., 2021; 2022). The observed correlation (RDA analysis; Fig. 7) between TOC, TN and diatom frustules also suggests that phytodetritus is one of the sources of organic matter in the shelf sediment and is consistent with our previous observation. The distribution of diatom and organic matter revealed a strong spatial variability. Usually, the mass production of diatoms in the Eastern Arabian Sea is closely related to the nutrient supply to the euphotic layers by atmospheric forcing (Habeebrehman et al., 2008; Albin et al., 2022; Chowdhury and Biswas, 2023). Likewise, high absolute abundance of diatom frustules at the southern (15° N >11° N) and the northern (21° N) sites mostly originated from diatom blooms induced by upwelling and winter convection, respectively (Fig. 1A, B, C). Nevertheless, as the surface sediment represents a mixture of phytodetritus accumulated over the years, it is difficult to delineate seasonal fluxes of organic matter or diatom frustules particularly in the case of slow sedimentation rates.

Furthermore, the preservation/loss of organic matter and frustules depends on the geochemical properties of the sediments, the oxygen content, and the size and thickness of diatom frustules. Therefore, the diversity of diatom assemblages observed in the surface sediment could be partly attributed to their preservation potential. To establish this fact, the sedimentary diatom diversity was compared with the diversity from the overlying water column reported in various literature from this region (Table 5). It was observed that not all bloom-forming diatoms are preserved in the sediment. The dead frustule can dissolve quite rapidly, even within hours to days (Kamatani and Riley, 1979), depending on temperature, pH, dissolved oxygen levels, heterotrophic activity, (Lewin, 1961), including the gradient in DSi levels between the sediments, and the overlying water column. It has been shown that at higher temperatures (> 20° C) and pH, biogenic silica can be dissolved relatively mre rapidly

than in cold water and at low pH (Roubeix et al., 2008). Recently, a synthesis of a large-scale mesocosm study showed that low pH slows the dissolution of dead frustules (Taucher et al., 2022) and vice versa. However, frustules build up resistance to dissolution by forming an organic matrix (Lewin, 1961) that can be degraded by microbial activity leading to dissolution (Bidle and Azam, 1999; Roubeix et al., 2008). A similar trend was observed by Pandey et al. (2023) in the surface sediments of the north-central Arabian Sea (19–21°N, 64° E), showing that the presence of a thick OMZ (about 1000 m) facilitated higher diatom flux and preservation compared to the regions (11–13°N, 64° E) where the OMZ was relatively thinner (~400 m) (Fig. 1A). The presence of the OMZ along the shelf and its spatial variability (intensified towards the north, while negligible in the south) may be a crucial factor in organic matter preservation and is discussed in the following sections.

4.1 Geochemical characteristics of sediment

The average organic carbon content of the surface sediments was found to be quite high (18.8 mg g^{-1}), reaching a maximum of 3.4% at 15° N (Fig. 6B; Table 2). In the Eastern Arabian Sea, shelf and slope sediments (up to ~1000 m) are overlain by OMZ waters (Naqvi, 1994), which enhance organic carbon preservation. From a multi-proxy study from the Arabian Sea (Keil et al. 2016), it has been hypothesized that organic matter preservation and transfer may be efficient within the OMZ due to multiple factors including oxygen availability, carbon addition through the microbial loop, zooplankton abundance and activity , etc. Likewise, the significant positive correlation between TOC and TN contents also suggested a well-preserved status of the sediment organic matter (Supplementary Fig. 1F). The sediments of the productive shelf areas of the Eastern Arabian Sea have been reported to contain high TOC values with total organic matter of 22.8 mg g^{-1} corresponding to ~4% (Paropkari et al., 1992; Suthhof et al., 2000), which is comparable to our observation. Contrarily, the TOC content in the shelf region of the Bay of Bengal, the twin basin of the Arabian Sea, was found to be much lower (0.63 to 1.64% within the depth of 25 -1000 m) than these values (Krishna et al. 2013). It was previously reported that the organic-rich band in the shelf of the eastern Arabian Sea extending from Mumbai to the southern tip of India widens between 17 and 13° N (Paropkari et al., 1992), supporting the observation of high TOC contents. Particularly the highest TOC contents at 15° N could be attributed to the prevalence of OMZ from a depth of ~130 m (110 m in summer and 150 m in winter) to the sediment-water interface (Sudheesh et al. 2022), which limits the loss of organic matter via mineralization (Keil et al. 2016). On the other hand, the northern boundary of OMZ may touch 21° N (Fig. 1A) but remains narrower compared to 15° N (Sudheesh et al. 2022), resulting in less efficient carbon transport and preservation.

The influence of the OMZ at 11° N is the least and hence despite the high flux of phytodetritus as indicated by the maximum diatom valve flux, more oxygen availability could lead to loss of organic matter resulting in lower TOC, TN, and frustule numbers. This also explains the low diatom abundance at 11° N indicating a substantial loss of frustules by dissolution despite a fourfold higher diatom valve flux compared to the stations within the OMZ. The lowest frustule abundance and diversity at 19° N could be attributed to frustule dissolution, either due to more oxic conditions or calcareous (83.6% CaCO3; Table 2) sediment (alkaline sediment helps to dissolve opal faster, Zhang et al. 2015) compared to other stations. The highest TIC values at 19° N (Fig. 6A) could be attributed to the geomorphology of this region. The Fifty-Fathom-Flat is one of the prominent features along the Western Indian shelf occurring at 19° N (off Mumbai) and is usually dominated by carbonate

sands composed of oolites, foraminifers, coral fragments, and limestone (Nair, 1971). Blooms of calcifying nanoplankton (coccolithophores) have been documented in this location from both nutrient-poor surface waters (Chowdhury et al., 2022), and surface sediments (Andruleit et al., 2004). Studies of sediment trap samples from the Eastern Arabian Sea during the Joint Global Ocean Flux Studies (JGOFS) reported higher fluxes of carbonate (35% - 65%) containing nanoplanktonic coccolithophores and foraminifers (Ramaswamy and Nair, 1994) compared to organic carbon (3.8 –10 %) (Nair et al., 1989). The abundance of foraminifera (Rixen et al., 2005) has also been reported from sediment trap samples in nearby locations and may explain the presence of calcium carbonate-rich sediments with higher TIC contents.

4.2 Diversity of diatom frustules and the related processes

The average cell size of the phytoplankton could be an indication of the prevailing nutrient status. Overall size classes of the diatom frustules belonged to the medium (53%) and small (39%) categories (Supplementary Figure 1B) compared to the large frustules (8%), suggesting a moderately nutrient-enriched environment. This is because the ratio of surface area to volume increases with decreasing cell size, allowing higher nutrient uptake by the cell surface and vice versa (Marañón, 2015). Thus, moderate nutrient levels in any aquatic region can support the growth of medium-sized phytoplankton, contrary to the large cells that need a substantial amount of nutrients, (Marañón, 2015). Diatoms proliferate well under dissolved silica (DSi) enrichment, especially in coastal waters (Tréguer and De La Rocha, 2013). Abrantes et al (2016) noticed a positive exponential correlation between the DSi levels in the water column and the abundance of diatom valve in the sediment. Moreover, depletion of DSi (<2 µM) can promote small diatoms with thinner frustules as well as a community shift from diatoms to non-diatoms (Egge and Aksnes, 1992). Along the present study site, DSi levels do not remain high in the mixed layers except during upwelling and winter convection (3–4 µM, within the mixed layers; Albin et al., 2022; Chowdhury and Biswas, 2023) in the shelf waters and could therefore, support the moderate cell size diatoms. In a study by Sherin et al. (2023) covering the entire shelf for all seasons, it was observed that DSi levels were in generally higher towards the northern shelf (6.1 ±2.7 µM), whereas values between 1 -4 µM were observed in the southern and central part of the shelf. During the fall intermonsoon and premonsoon seasons, the nutrient levels (nitrate, phosphate, and DSi) can be quite low throughout the shelf region (Sherin et al. 2023) with low phytoplankton biomass. Such a gradient in nutrient availability from south to north, as well as seasonal variability seemed to directly influence the frustule size of diatoms.

The diatom taxon *Thalassiosira* (Cleve) Hasle was present in all stations with the highest contribution at 11 °N followed by 15° N (Fig. 2), with a gradual decrease towards the north. *Thalassiosira* is usually found in the core of upwelling regions where nutrients and turbulence are high and persistent (Abrantes, 1988), so , this trend could be partly attributed to the occurrence of intense upwelling in the south, supporting high nutrient levels for a prolonged period, but weakening toward the north (Banse, 1968). There are a few other facts that may also support this observation. For example, the export of *Thalassiosira* valves to the sediment could be facilitated by the formation of chains. It was also argued by some authors that chained cells may sink into the sediment more efficiently than solitary cells (Smayda, 1970; Waite et al., 1997). Their thick frustules may provide an advantage of better preservation and faster settling compared to thinly silicified cells like *Chaetoceros* sp., *Leptocylindrus* sp., and *Skeletonema* sp.

Another small centric diatom *Cyclotella* was observed only at southern stations (11–13° N) with the highest abundance at 13° N (Fig. 2), and has been reported to prefer low salinity waters (Tuchman et al., 1984). The southwestern shelf receives low salinity waters due to oceanic precipitation, river runoff during the summer monsoon, and the intrusion of low salinity Bay of Bengal waters carried by the West India Coastal Current during winter (Prasanna Kumar et al., 2004; Silori et al., 2022). During the summer monsoon, the average salinity within the mixed layer could be 34.7 at 8–12° N, and nearly 2 units higher values can be seen in the north (17–21° N) (Silori et al., 2022; Chowdhury and Biswas, 2023). Similarly, during the winter monsoon, salinity was reported to be >36 in the north, which was 2 units lower than in the southern shelf (8–12° N) (Vijayan et al., 2021; Albin et al., 2022). Thus, in the north, the prevalence of high salinity waters throughout the year could justify the absence of *Cyclotella*.

Coscinodiscus, a large centric diatom, was the second most abundant genus found in all stations with higher abundance towards north of 15° N (Fig. 2). This genus often dominates nutrient-rich waters enriched with DSi and dissolved inorganic nitrogen during upwelling and winter convection in this region (Madhupratap et al., 1996; Sawant and Madhupratap, 1996; Gauns et al., 2005; Habeebrehman et al., 2008; Chowdhury et al., 2021; Albin et al., 2022., Sathish et al., 2022). *Coscinodiscus* and *Rhizosolenia* blooms have been documented (Chowdhury et al., 2021) during open-ocean upwelling from the north-central Arabian Sea along 64 °E (Fig. 1A), and higher abundances of these frustules have also been found in surface sediments from these locations (Pandey et al., 2023; Pandey et al 2024). In the western Arabian Sea, Koning et al. (2001) observed *Coscinodiscus*, *Proboscia*, and *Rhizosolenia* in the water column during the upwelling and later in the sediment trap as well as in the surface sediment when upwelling ceased. Taken together, these observations explain the high abundance of *Coscinodiscus* in the northern shelf regions. However, the lower abundance of *Coscinodiscus* in the southern shelf region needs further explanation.

A predominant reason may be its removal via grazing by zooplankton and planktivorous fishes (Madhupratap et al., 1990; Padmavati et al., 1998) that may remove a substantial portion of phytoplankton biomass from the water column before it reaches the sediment. Particularly due to the dominance of herbivorous copepods and planktivorous fishes like Oil Sardines in these regions (Madhupratap et al., 1990; Padmavati et al., 1998; Jyothibabu et al., 2010). Jagadeesan et al. (2017) reported a 14.2% removal of phytoplankton standing stock by calanoid copepods in the southwest coast of India during the pre-monsoon months and this value increased to 50% during the summer-monsoon and post-monsoon. Gut content analysis of Indian Oil Sardines and mackerels revealed the presence of a substantial proportion (>80%) of phytoplankton standing stock dominated by *Fragilaria oceanica*, *Coscinodiscus*, *Thalassiosira*, *Nitzschia, Pleurosigma, Chaetoceros, Cyclotella,* and *Thalassionema* (Subrahmanyan, 1959; Remya et al., 2013; Nair et al., 2023). Interestingly, it was observed that during pre-monsoon months (May), the guts of Indian Oil Sardine collected from the southwest coast of India were partly filled (~9%) with large *Coscinodiscus* and *Biddulphia* (Noble, 1964). But, during the peak monsoon months (July –September), the guts of Sardines were mostly filled (50 -90%) with *Coscinodiscus*.

In contrast, on the northern shelf, the dominance of carnivorous fishes may not remove much of the phytoplankton standing stock and thus may be advantageous for *Coscinodiscus*. Moreover, large and highly silicified cells like *Coscinodiscus* and *Rhizosolenia,* which grow at high nutrient levels during convective mixing, may be less preferred for grazing as they are difficult to crush (Hamm et al., 2003; Ryderheim et al., 2022) and may sink to the seabed.

The pennate diatom *Nitzschia* was the third most abundant diatom with the highest relative abundance at 15° N (Fig. 2). This genus is commonly found in southwestern Indian shelf waters (8–17° N) (Ahmed et al., 2016; Karnan et al., 2020; Albin et al., 2022), which may be due to its small size, which helps it to grow even at low nutrient levels (Marañón, 2015). Desikachary (1989) also reported significant occurrences of *Nitzschia* frustules in the surface sediments of the Indian Ocean. High abundances of *Fragilaria* and *Fragilariopsis* were noticed from the southern shelf (Fig. 2), as these species have been identified as bloom formers in upwelling areas as reported in previous studies (Nair and Subrahmanyan, 1955; Jyothibabu et al., 2018). The diatoms *Thalassionema*, *Pseudo-nitzschia,* and *Navicula* showed the highest abundances at stations 15 and 21° N (Fig. 2), and like *Nitzschia* they can be generalists that thrive well in the continental margin waters (Cloern and Dufford, 2005). However, some small-sized diatoms (e.g. *Nitzschia*, *Pseudo-nitzschia*) can produce certain toxins to prevent grazing (Harðardóttir et al., 2019) and can be exported to the sediment as found in the present study. Chain formation may also facilitate their export to the sediment (Smayda, 1970; Waite et al., 1997). Thus, different adaptive strategies of diatoms to avoid grazing could facilitate their transport to the sediment. These species may have a higher preservation potential to remain in the sediment for a longer periods of time and have also been reported from the sediments of the South China Sea (Ran et al., 2024).

The two thinly silicified centric diatoms *Chaetoceros* and *Cerataulina* bloom during the upwelling season, particularly in the south, with decreasing abundance northwards of the Indian shelf (Chowdhury and Biswas, 2023 and references therein). *Chaetoceros* could be competitively superior to *Thalassiosira* in bloom formation when turbulence due to upwelling ceases (Kemp and Villareal, 2018) and is usually observed in higher abundance during the later stages of upwelling (Thomas et al., 2013; Chowdhury and Biswas, 2023). The absence of intact frustules of these genera in our samples may be due to removal by grazing or to their weakly silicified frustules, which are prone to dissolution. Noble (1964) observed that a large number of *Chaetoceros* were found in the gut contents of Indian Oil Sardines during the post-monsoon period (October and December). Interestingly, the resting spores of *Chaetoceros* and *Cerataulina* were found in the shelf sediment to the south (Table 3), which is affected by upwelling. Some diatoms can survive for long periods by forming resting spores under unfavorable growth conditions (Kitchell et al., 1986) and germinate when the conditions are reversed (Sanyal et al., 2021). In several oceanographic regions, these resting spores contribute a substantial part of the sedimentary diatom assemblages (Pitcher, 1986). For example, in the Somali upwelling region, a high flux of *Chaetoceros* resting spores was observed after the summer monsoon upwelling-induced bloom (Koning et al., 2001). In some studies, *Chaetoceros* resting spore abundance was found to be positively correlated with low salinity (Sanyal et al., 2021). However, this may not justify the trend observed in this study. *Cerataulina* resting spores have been also reported from surface sediments of a tropical estuarine system on the northeast coast of India with a wide range of salinities (Sarkar et al., 2024).

5.1 Conclusion

This study analyzed organic matter (TOC, TN) along with diatom frustules (abundance, distribution, and diversity) from surface sediments of the western Indian continental shelf. The ^{210}Pb analysis indicated a relatively recent signature (~ 4.5 years) of phytodetritus. The content of organic matter was found to be relatively high (~4%) suggesting a well-preserved signature and can be due to the influence of the OMZ along this shelf region. The highest diatom valve flux was noticed in the upwelling-impacted station (11° N), however, frustule number, diversity, and organic matter (TOC, TN) remained low and could be attributed to loss due to mineralization. On

the other hand, the station under the influence of the OMZ and weak upwelling was associated with moderate diatom valve flux but the highest organic matter content and frustule numbers and diversity. Overall, the results indicate a substantial loss of frustules due to dissolution and that some taxa are efficient in preservation. Two centric (*Thalassiosira, Coscinodiscus*) and one pennate (*Nitzschia*) diatoms contributed the most to the total diatom assemblages, and these diatoms were also frequently reported from the upper water column. Their frustule size, thickness, chain formation, and other relevant characteristics may explain their dominance in the sediments. In contrast, thinly silicified genera, such as *Chaetoceros* and *Leptocylindrus,* were not found in the surface sediment, although they are known to be abundant in the water column during the bloom. This could be due to the low preservation capacity of thin frustules or perhaps removal by grazing before reaching the sediment. Resting spores of *Chaetoceros* and *Cerataulina* were found in the stations impacted by upwelling. Future studies on export fluxes, rates, and mineralization of diatom-derived organic matter at the sediment-water interface are highly recommended, as such information is still scarce from this shelf region.

Acknowledgments

The first author acknowledges the Department of Science and Technology (DST) - Inspire for funding her fellowship. CSIR-NIO in-house program "Impact of Climate Change on the Physics, Biogeochemistry, and the Ecology of the North Indian Ocean (CliCNIO)" (MLP 1802) was funded by the Council of Scientific and Industrial Research. We thank the captain, scientists, technical staff, ship cell staff, deckhands, and the students onboard RV Sindhu Sadhana (SSD 068) for their constant help and support during the cruise. The Director, CSIR NIO is highly acknowledged for his help and support. Ms. Teja Naik and Mr. Areef Sardar are acknowledged for their help with the Coulometer and Scanning Electron Microscopy (SEM) respectively in CSIR, NIO. Radionuclide (^{210}Pb, ^{226}Ra) measurements were self-financed by Sabine Schmidt (EPOC). We are thankful to the anonymous reviewers for their constructive comments and suggestions. The NIO contribution number is XXXX.

Author Contributions*: MP: Conceptualization, sampling, formal analysis, data curation, writing original manuscript and editing; HB: Fund acquisition; sampling; manuscript reviewing and editing SS:Radionuclides analysis/interpretation and manuscript reviewing and editing.*

Fundings sources: The first author was funded by the Department of Science and Technology (DST) – Inspire, Government of India. ^{210}Pb measurements were self-financed by Sabine Schmidt (EPOC)

Statements and Declarations

Competing Interests*: The authors have no relevant financial or non-financial interests to disclose.*

Ethical Approval: Not applicable

Consent to Participate: Not applicable

Consent to Publish: Not applicable

Availability of data and materials: Data will be available on request.

References:

1. Abrantes, F., 1988. Diatom assemblages as upwelling indicators in surface sediments off Portugal. *Marine Geology*, *85*(1), 15-39.https://doi.org/10.1016/0025-3227(88)90082-5
2. Abrantes, F., Cermeno, P., Lopes, C., Romero, O., Matos, L., Van Iperen, J., Rufino, M., Magalhães, V., 2016. Diatoms Si uptake capacity drives carbon export in coastal upwelling systems. *Biogeosciences*, *13*(14), 4099-4109.https://doi.org/10.5194/bg-13-4099-2016
3. Abrantes, F., Meggers, H., Nave, S., Bollman, J., Palma, S., Sprengel, C., Henderiks, J., Spies, A., Salgueiro, E., Moita, T., Neuer, S., 2002. Fluxes of micro-organisms along a productivity gradient in the Canary Islands region (29 N): implications for paleo reconstructions. *Deep Sea Research Part II: Topical Studies in Oceanography*, *49*(17), 3599-3629.https://doi.org/10.1016/S0967-0645(02)00100-5
4. Abrantes, F.F.G., Sancetta, C., 1985. Diatom assemblages in surface sediments reflect coastal upwelling off southern Portugal. *Oceanologicaacta*, *8*(1), 7-12.
5. Ahmed, A., Kurian, S., Gauns, M., Chndrasekhararao, A.V., Mulla, A., Naik, B., Naik, H., Naqvi, S.W.A., 2016. Spatial variability in phytoplankton community structure along the eastern Arabian Sea during the onset of south-west monsoon. *Continental Shelf Research*, *119*, 30-39.https://doi.org/10.1016/j.csr.2016.03.005
6. Albin, K.J., Jyothibabu, R., Alok, K.T., Santhikrishnan, S., Sarath, S., Sudheesh, V., Sherin, C.K., Balachandran, K.K., Devi, C.A., Gupta, G.V.M., 2022. Distinctive phytoplankton size responses to the nutrient enrichment of coastal upwelling and winter convection in the eastern Arabian Sea. *Progress in Oceanography*, *203*, 102779.https://doi.org/10.1016/j.pocean.2022.102779
7. Andruleit, H., Rogalla, U. and Stäger, S., 2004. From living communities to fossil assemblages: origin and fate of coccolithophores in the northern Arabian Sea. *Micropaleontology*, *50*(Suppl_1), 5-21. https://doi.org/10.2113/50.Suppl_1.5
8. Armbrecht, L.H., Lowe, V., Escutia, C., Iwai, M., McKay, R., Armand, L.K., 2018. Variability in diatom and silicoflagellate assemblages during mid-Pliocene glacial-interglacial cycles determined in Hole U1361A of IODP Expedition 318, Antarctic Wilkes Land Margin. *Marine Micropaleontology*, *139*, 28-41.https://doi.org/10.1016/j.marmicro.2017.10.008
9. Banse, K., 1968, February. Hydrography of the Arabian Sea shelf of India and Pakistan and effects on demersal fishes. In *Deep sea research and oceanographic Abstracts* (Vol. 15, No. 1, 45-79). Elsevier.https://doi.org/10.1016/0011-7471(68)90028-4
10. Banse, K., 1990. New views on the degradation and disposition of organic particles as collected by sediment traps in the open sea. *Deep Sea Research Part A. Oceanographic Research Papers*, *37*(7), 1177-1195.https://doi.org/10.1016/0198-0149(90)90058-4
11. Banse, K., McClain, C.R., 1986. Winter blooms of phytoplankton in the Arabian Sea as observed by the Coastal Zone Color Scanner. *Marine Ecology Progress Series*, 201-211.https://doi.org/10.3354/meps034201
12. Bidle, K.D., Azam, F., 1999. Accelerated dissolution of diatom silica by marine bacterial assemblages. *Nature*, *397*(6719), 508-512.https://doi.org/10.1038/17351
13. Bjærke, O., Jonsson, P.R., Alam, A. and Selander, E., 2015. Is chain length in phytoplankton regulated to evade predation?. *Journal of Plankton Research*, 37(6), 1110-1119. https://doi.org/10.1093/plankt/fbv076

14. Cavan, E.L., Le Moigne, F.A., Poulton, A.J., Tarling, G.A., Ward, P., Daniels, C.J., Fragoso, G.M., Sanders, R.J., 2015. Attenuation of particulate organic carbon flux in the Scotia Sea, Southern Ocean, is controlled by zooplankton fecal pellets. *Geophysical Research Letters*, *42*(3),821-830.https://doi.org/10.1002/2014GL062744
15. Chowdhury, M., Biswas, H., 2023. A coherent status of summer monsoon phytoplankton communities (2017–2018) along the Western Indian continental shelf: Implications for fisheries. *Science of The Total Environment*, *878*, 162963.http://dx.doi.org/10.1016/j.scitotenv.2023.162963
16. Chowdhury, M., Biswas, H., Mitra, A., Silori, S., Sharma, D., Bandyopadhyay, D., Shaik, A.U.R., Fernandes, V., Narvekar, J., 2021. Southwest monsoon-driven changes in the phytoplankton community structure in the central Arabian Sea (2017–2018): After two decades of JGOFS. *Progress in Oceanography*, *197*, 102654.https://doi.org/10.1016/j.pocean.2021.102654
17. Chowdhury, M., Biswas, H., Sharma, D., Silori, S., Winter, A., 2022. Distribution of extant coccolithophores from the northwest continental shelf of India during the summer monsoon. *Phycologia*, *61*(3), 284-298.https://doi.org/10.1080/00318884.2022.2037340
18. Cloern, J.E., Dufford, R., 2005. Phytoplankton community ecology: principles applied in San Francisco Bay. *Marine Ecology Progress Series*, *285*, 11-28.https://doi.org/10.3354/meps285011
19. De La Rocha, C.L., Nowald, N., Passow, U., 2008. Interactions between diatom aggregates, minerals, particulate organic carbon, and dissolved organic matter: Further implications for the ballast hypothesis. *Global Biogeochemical Cycles*, *22*(4):1-10.https://doi.org/10.1029/2007GB003156
20. Desikachary, T.V., 1989. Atlas of Diatoms (Marine Diatoms of the Indian Ocean Region). 6. Madras Science Foundation, Madras Fasc, 1–13
21. Falkowski, P.G., Flagg, C.N., Rowe, G.T., Smith, S.L., Whitledge, T.E., Wirick, C.D., 1988. The fate of a spring phytoplankton bloom: export or oxidation?. *Continental Shelf Research*, *8*(5-7), 457-484.https://doi.org/10.1016/0278-4343(88)90064-7
22. Gauns, M., Madhupratap, M., Ramaiah, N., Jyothibabu, R., Fernandes, V., Paul, J.T., Kumar, S.P., 2005. Comparative accounts of biological productivity characteristics and estimates of carbon fluxes in the Arabian Sea and the Bay of Bengal. *Deep Sea Research Part II: Topical Studies in Oceanography*, *52*(14-15), 2003-2017.https://doi.org/10.1016/j.dsr2.2005.05.009
23. Gopinathan, C.P., Gireesh, R., Smitha, K.S., 2001. Distribution of chlorophyll 'a' and 'b' in the eastern Arabian Sea (west coast of India) in relation to nutrients during postmonsoon. *Journal of the Marine Biological Association of India*, *43*(1 and 2), 21-30.
24. Habeebrehman, H., Prabhakaran, M.P., Jacob, J., Sabu, P., Jayalakshmi, K.J., Achuthankutty, C.T., Revichandran, C., 2008. Variability in biological responses influenced by upwelling events in the Eastern Arabian Sea. *Journal of Marine Systems*, *74*(1-2), 545-560.https://doi.org/10.1016/j.jmarsys.2008.04.002
25. Hamm, C.E., Merkel, R., Springer, O., Jurkojc, P., Maier, C., Prechtel, K.,Smetacek, V., 2003. Architecture and material properties of diatom shells provide effective mechanical protection. *Nature*, *421*(6925), 841-843.https://doi.org/10.1038/nature01416
26. Harðardóttir, S., Wohlrab, S., Hjort, D.M., Krock, B., Nielsen, T.G., John, U., Lundholm, N., 2019. Transcriptomic responses to grazing reveal the metabolic pathway leading to the biosynthesis of domoic acid

and highlight different defense strategies in diatoms. *BMC molecular biology*, *20*(1), 1-14.https://doi.org/10.1186/s12867-019-0124-0

27. Harrison, P.J., Zingone, A., Mickelson, M.J., Lehtinen, S., Ramaiah, N., Kraberg, A.C., Sun, J., McQuatters-Gollop, A. and Jakobsen, H.H., 2015. Cell volumes of marine phytoplankton from globally distributed coastal data sets. Estuarine, *Coastal and Shelf Science*, 162, 130-142. https://doi.org/10.1016/j.ecss.2015.05.026
28. Hedges, J.I., Keil, R.G., 1995. Sedimentary organic matter preservation: an assessment and speculative synthesis. *Marine chemistry*, *49*(2-3), 81-115.https://doi.org/10.1016/0304-4203(95)00008-F
29. Jagadeesan, L., Jyothibabu, R., Arunpandi, N. and Parthasarathi, S., 2017. Copepod grazing and their impact on phytoplankton standing stock and production in a tropical coastal water during the different seasons. Environmental monitoring and assessment, 189, pp.1-21. https://doi.org/10.1007/s10661-017-5804-y
30. Jyothibabu, R., Arunpandi, N., Karnan, C., Jagadeesan, L., Manojkumar, T.M., Balachandran, K.K., Naqvi, S.W.A., 2018. Fragilariopsis sp. bloom causes yellowish-brown waters off Alappuzha, south-central Kerala coast, India, during the mud bank-upwelling phase. *Current Science*, *115*(1), 152-159.
31. Jyothibabu, R., Chinnadurai, K., Loganathan, J.,Nagarathinam, A., Singaram, P., Jose, A.K., 2021. Ecological responses of autotrophic microplankton to the eutrophication of the coastal upwelling along the Southwest coast of India. *Environmental Science and Pollution Research*, *28*, 11401-11414.https://doi.org/10.1007/s11356-020-11354-2
32. Jyothibabu, R., Madhu, N.V., Habeebrehman, H., Jayalakshmy, K.V., Nair, K.K.C., Achuthankutty, C.T., 2010. Re-evaluation of 'paradox of mesozooplankton' in the eastern Arabian Sea based on ship and satellite observations. *Journal of Marine Systems*, *81*(3), 235-251.https://doi.org/10.1016/j.jmarsys.2009.12.019
33. Kamatani, A., Riley, J.P., 1979. Rate of dissolution of diatom silica in seawater. *Mar Biol*, *55*, 29-35.https://doi.org/10.1007/BF00391714
34. Karnan, C., Jyothibabu, R., Arunpandi, N., Albin, K.J., Parthasarathi, S., Krishnan, S.S., 2020. Response of microplankton size structure to summer stratification, freshwater influx and coastal upwelling in the Southeastern Arabian Sea. *Continental Shelf Research*, *193*, 104038.https://doi.org/10.1016/j.csr.2019.104038
35. Keil, R.G., Neibauer, J.A., Biladeau, C., van der Elst, K.,Devol, A.H., 2016. A multiproxy approach to understanding the" enhanced" flux of organic matter through the oxygen-deficient waters of the Arabian Sea. *Biogeosciences*, *13*(7),2077-2092.https://doi.org/10.5194/bg-13-2077-2016
36. Kitchell, J.A., Clark, D.L. and Gombos Jr, A.M., 1986. Biological selectivity of extinction: a link between background and mass extinction. *Palaios*, 504-511. https://doi.org/10.2307/3514632
37. Koizumi, I., 1985. Neogene diatom biostratigraphy of the middle latitude western north Pacific, Deep Sea Drilling Project Leg 86. *Init. Repts. Deep Sea Drilling Project*, *86*, 269-300.
38. Koning, E., Van Iperen, J.M., Van Raaphorst, W., Helder, W., Brummer, G.J. and Van Weering, T.C.E., 2001. Selective preservation of upwelling-indicating diatoms in sediments off Somalia, NW Indian Ocean. *Deep Sea Research Part I: Oceanographic Research Papers*, *48*(11), 2473-2495. https://doi.org/10.1016/S0967-0637(01)00019-X .
39. Krishna, M.S., Naidu, S.A., Subbaiah, C.V., Sarma, V.V.S.S. and Reddy, N.P.C., 2013. Distribution and sources of organic matter in surface sediments of the eastern continental margin of India. *Journal of Geophysical Research: Biogeosciences*, *118*(4), pp.1484-1494. https://doi.org/10.1002/2013JG002424

40. Kuwae, M., Yamashita, A., Hayami, Y., Kaneda, A., Sugimoto, T., Inouchi, Y., Amano, A. and Takeoka, H., 2006. Sedimentary records of multidecadal-scale variability of diatom productivity in the Bungo Channel, Japan, associated with the Pacific Decadal Oscillation. Journal of oceanography, 62, 657-666. https://doi.org/10.1007/s10872-006-0084-0
41. Lampitt, R.S., 1985. Evidence for the seasonal deposition of detritus to the deep-sea floor and its subsequent resuspension. *Deep Sea Research Part A. Oceanographic Research Papers*, *32*(8), 885-897.https://doi.org/10.1016/0198-0149(85)90034-2
42. Le Moigne, F.A., Henson, S.A., Cavan, E., Georges, C., Pabortsava, K., Achterberg, E.P., Ceballos-Romero, E., Zubkov, M., Sanders, R.J., 2016. What causes the inverse relationship between primary production and export efficiency in the Southern Ocean?. *Geophysical Research Letters*, *43*(9), 4457-4466.https://doi.org/10.1002/2016GL068480
43. Le Moigne, F.A., Poulton, A.J., Henson, S.A., Daniels, C.J., Fragoso, G.M., Mitchell, E., Richier, S., Russell, B.C., Smith, H.E., Tarling, G.A., Young, J.R., 2015. Carbon export efficiency and phytoplankton community composition in the A tlantic sector of the A rctic Ocean. *Journal of Geophysical Research: Oceans*, *120*(6), 3896-3912.https://doi.org/10.1002/2015JC010700
44. Lewin, J.C., 1961. The dissolution of silica from diatom walls. *GeochimicaetCosmochimicaActa*, *21*(3-4), 182-198.https://doi.org/10.1016/S0016-7037(61)80054-9
45. Liu, T., Qiu, Y., Lin, X., Ni, X., Wang, L., Li, H., & Jing, C. (2024). Dissolved oxygen recovery in the oxygen minimum zone of the Arabian Sea in recent decade as observed by BGC-argo floats. Geophysical Research Letters, 51(12), e2024GL108841. https://doi.org/10.1029/2024GL108841
46. Madhupratap, M., Haridas, P., 1990. Zooplankton, especially calanoid copepods, in the upper 1000 m of the south-east Arabian Sea. *Journal of Plankton Research*, *12*(2), 305-321.https://doi.org/10.1093/plankt/12.2.305
47. Madhupratap, M., Kumar, S.P., Bhattathiri, P.M.A., Kumar, M.D., Raghukumar, S., Nair, K.K.C.,Ramaiah, N., 1996. Mechanism of the biological response to winter cooling in the northeastern Arabian Sea. *Nature*, *384*(6609),549-552.https://doi.org/10.1038/384549a0
48. Marañón, E., 2015. Cell size as a key determinant of phytoplankton metabolism and community structure. *Annual Rereview of Mmarine scienceScience*, *7*, 241-264.https://doi.org/10.1146/annurev-marine-010814-015955
49. Nair, P.G., Joseph, S., Pillai, N., Abdulla, M.H.A., 2023. Is there a significant long-term shift in phytoplankton in small pelagic fish diets along India's southwest coast? *Oceanologia*, *65*(2), 297-309.https://doi.org/10.1016/j.oceano.2022.07.001
50. Nair, R.R., 1971, March. Beachrock and associated carbonate sediments on the Fifty Fathom Flat, a submarine terrace on the outer continental shelf off Bombay. In *Proceedings/Indian Academy of Sciences* (Vol. 73, No. 3, 148-154). New Delhi: Springer India.https://doi.org/10.1007/BF0304531
51. Nair, R.R., Ittekkot, V., Manganini, S.J., Ramaswamy, V., Haake, B., Degens, E.T., Desai, B.T., Honjo, S., 1989. Increased particle flux to the deep ocean related to monsoons. *Nature*, *338*(6218), 749-751.https://doi.org/10.1038/338749a0
52. Nair, R.V., Subrahmanyan, R., 1955. The diatom, Fragilaria oceanica Cleve, an indicator of abundance of the Indian oil sardine, SardinellalongicepsCuv. and Val. *Current Science*, *24*(2), 41-42.

53. Naqvi, S.W.A., 1994. Denitrification processes in the Arabian Sea. *Proceedings of the Indian Academy of Sciences-Earth and Planetary Sciences*, 103, 279-300. https://doi.org/10.1007/BF02839539
54. Naqvi, S.W.A., Noronha, R.J., Somasundar, K., Gupta, R.S., 1990. Seasonal changes in the denitrification regime of the Arabian Sea. *Deep Sea Research Part A. Oceanographic Research Papers*, *37*(4), 593-611.https://doi.org/10.1016/0198-0149(90)90092-A
55. Naqvi, W.A., 1991. Geographical extent of denitrification in the Arabian Sea in relation to some physical processes. *Oceanologica Acta*, *14*(3), 281-290.
56. Noble, A., 1964. Food and feeding habits of the Indian oil sardine Sardinella longiceps Valenciennes at Karwar. Indian Journal of Fisheries, 12(1), pp.77-87.
57. Padmavati, G., Haridas, P., Nair, K.K.C., Gopalakrishnan, T.C., Shiney, P., Madhupratap, M., 1998. Vertical distribution of mesozooplankton in the central and eastern Arabian Sea during the winter monsoon. *Journal of Plankton Research*, *20*(2), 343-354.https://doi.org/10.1093/plankt/20.2.343
58. Pandey, M., Biswas, H., Chowdhury, M., 2023. Interlinking diatom frustule diversity from the abyss of the central Arabian Sea to surface processes: physical forcing and oxygen minimum zone. *Environmental Monitoring and Assessment*, *195*(1), 161.https://doi.org/10.1007/s10661-022-10749-7
59. Pandey, M., Biswas, H., Birgel, D., Burdanowitz, N. and Gaye, B., 2024. Sedimentary organic matter signature hints at the phytoplankton-driven biological carbon pump in the central Arabian Sea. Biogeosciences, 21(20), pp.4681-4698. https://doi.org/10.5194/bg-21-4681-2024
60. Parab, S.G.,Matondkar, S.P., Gomes, H.D.R., Goes, J.I., 2006. Monsoon driven changes in phytoplankton populations in the eastern Arabian Sea as revealed by microscopy and HPLC pigment analysis. *Continental Shelf Research*, *26*(20), 2538-2558.https://doi.org/10.1016/j.csr.2006.08.004
61. Paropkari, A.L., Babu, C.P. and Mascarenhas, A., 1993. New evidence for enhanced preservation of organic carbon in contact with oxygen minimum zone on the western continental slope of India. Marine Geology, 111(1-2), 7-13. https://doi.org/10.1016/0025-3227(93)90185-X
62. Paropkari, A.L., Babu, C.P., Mascarenhas, A., 1992. A critical evaluation of depositional parameters controlling the variability of organic carbon in Arabian Sea sediments. *Marine Geology*, *107*(3), 213-226.https://doi.org/10.1016/0025-3227(92)90168-H
63. Pitcher, G.C., 1986. Sedimentary flux and the formation of resting spores of selected Chaetoceros species at two sites in the southern Benguela system. *South African Journal of Marine Science*, 4(1), 231-244. https://doi.org/10.2989/025776186784461657
64. Prasanna Kumar S., Madhupratap, M., Kumar, M.D., Gauns, M., Muraleedharan, P.M., Sarma, V.V.S.S., De Souza, S.N., 2000. Physical control of primary productivity on a seasonal scale in central and eastern Arabian Sea. *Journal of Earth System Science*, *109*, 433-441.https://doi.org/10.1007/BF02708331
65. Prasanna Kumar, S., Narvekar, J., Kumar, A., Shaji, C., Anand, P., Sabu, P., Rijomon, G., Josia, J., Jayaraj, K.A., Radhika, A., Nair, K.K.C., 2004. Intrusion of the Bay of Bengal water into the Arabian Sea during winter monsoon and associated chemical and biological response. *Geophysical Research Letters*, *31*(15).https://doi.org/10.1029/2004GL020247
66. Ramaswamy, V., Nair, R.R., 1994. Fluxes of material in the Arabian Sea and Bay of Bengal—Sediment trap studies. *Proceedings of the Indian Academy of Sciences-Earth and Planetary Sciences*, *103*, 189-210.

67. Ran, L., Wiesner, M.G., Liang, Y., Liang, W., Zhang, L., Yang, Z., Li, H. and Chen, J., 2024. Differential dissolution of biogenic silica significantly affects the utility of sediment diatoms as paleoceanographic proxies. *Limnology and Oceanography*. https://doi.org/10.1002/lno.12492
68. Remya, R., Vivekanandan, E., Manjusha, U., Nair, P.G., 2013. Seasonal variations in the diet of the Indian oilsardine, SardinellalongicepsValenciennes off Cochin, Kerala. *Indian Journal of Fisheries*, *60*(1), 55-59.
69. Rixen, T., Guptha, M.V.S., Ittekkot, V., 2005. Deep ocean fluxes and their link to surface ocean processes and the biological pump. *Progress in Oceanography*, *65*(2-4), 240-259.https://doi.org/10.1016/j.pocean.2005.03.006
70. Roubeix, V., Becquevort, S., Lancelot, C., 2008. Influence of bacteria and salinity on diatom biogenic silica dissolution in estuarine systems. *Biogeochemistry*, *88*, 47-62.https://doi.org/10.1007/s10533-008-9193-8
71. Ryderheim, F., Grønning, J. and Kiørboe, T., 2022. Thicker shells reduce copepod grazing on diatoms. *Limnology and Oceanography Letters*, *7*(5),435-442. https://doi.org/10.1002/lol2.10243
72. Sanyal, A., Larsson, J., van Wirdum, F., Andrén, T., Moros, M., Lönn, M. and Andrén, E., 2022. Not dead yet: Diatom resting spores can survive in nature for several millennia. *American Journal of Botany*, *109*(1), 67-82. https://doi.org/10.1002/ajb2.1780
73. Sarkar, N.S, Biswas, B., Mandal, M., Das, T. and Sekh, S., 2024. Prevalence history of morphological variants of Cerataulina resting spores in Indian Sundarbans and resultant phylogenetic analysis. *Botanica Marina,* (0). https://doi.org/10.1515/bot-2023-0034
74. Sathish, T., VM, M.L., Thomas, L.C., Kuttippurath, J., Padmakumar, K.B., 2022. Spatial variability in the community structure of microphytoplankton along the southeastern Arabian sea during an unusually warm winter monsoon season. *Regional Studies in Marine Science*, *49*, 102078.https://doi.org/10.1016/j.rsma.2021.102078
75. Sawant, S., Madhupratap, M., 1996. Seasonality and composition of phytoplankton. *Current Science*, *71*(11).
76. Schmidt S., Howa H., Diallo A., Martín J., Cremer M., Duros P., Fontanier Ch., Deflandre B., Metzger E. & Mulder Th. (2014) Recent sediment transport and deposition in the Cap-Ferret Canyon, South-East margin of Bay of Biscay. Deep Sea Research II 104, 134-144. https://doi.org/10.1016/j.dsr2.2013.06.004
77. Scharek, R., Tupas, L. M., & Karl, D. M. (1999). Diatom fluxes to the deep sea in the oligotrophic North Pacific gyre at Station ALOHA. Marine Ecology Progress Series, 182, 55-67. doi:10.3354/meps182055
78. Schuette, G., Schrader, H., 1981. Diatoms in surface sediments: a reflection of coastal upwelling. *Coastal upwelling*, *1*, 372-380.https://doi.org/10.1029/CO001p0372
79. Shah, P., Sajeev, R. and Gopika, N., 2015. Study of upwelling along the west coast of India—A climatological approach. *Journal of Coastal Research*, *31*(5), 1151-1158. https://doi.org/10.2112/JCOASTRES-D-13-00094.1
80. Shankar, D. and Shetye, S.R., 1997. On the dynamics of the Lakshadweep high and low in the southeastern Arabian Sea. *Journal of Geophysical Research: Oceans*, 102(C6), 12551-12562. https://doi.org/10.1029/97JC00465
81. Shannon, C.E., Weaver, W., 1963. The Mathematical Theory of Communication. University of Illinois Press, Urbana.
82. Sherin, C.K., Gupta, G.V.M., Sudheesh, V., Ramu, C.V., Reddy, B., Harikrishnachari, N.V. and Vijayan, A.K., 2023. Nutriclines and nutrient stoichiometry in the eastern Arabian Sea: Intra-annual variations and

controlling mechanisms. Progress in Oceanography, 215, p.103048. https://doi.org/10.1016/j.pocean.2023.103048

83. Shetye, S.R., Gouveia, A.D. and Shenoi, S.S.C., 1994. Circulation and water masses of the Arabian Sea. *Proceedings of the Indian Academy of Sciences-Earth and Planetary Sciences*, 103, 107-123.
84. Shetye, S.R., Gouveia, A.D., Shenoi, S.S.C., Sundar, D., Michael, G.S., Almeida, A.M., Santanam, K., 1990. Hydrography and circulation off the west coast of India during the southwest monsoon 1987. *Journal of Marine Research*, *48*(2), 359-378.https://doi.org/10.1357/002224090784988809
85. Silori, S., Biswas, H., Chowdhury, M., Sharma, D., Magloire, M.Y., Cardinal, D., 2022. Interannual variability in particulate organic matter distribution and its carbon stable isotope signatures from the western Indian shelf waters. *Science of The Total Environment*, *844*, 157044.https://doi.org/10.1016/j.scitotenv.2022.157044
86. Silori, S., Sharma, D., Chowdhury, M., Biswas, H., Bandyopadhyay, D., Shaik, A.U.R., Cardinal, D., Mandeng-Yogo, M., Narvekar, J., 2021. Contrasting phytoplankton and biogeochemical functioning in the eastern Arabian Sea shelf waters recorded by carbon isotopes (SW monsoon). *Marine Chemistry*, *232*, 103962.https://doi.org/10.1016/j.marchem.2021.103962
87. Smayda, T.J., 1970. The suspension and sinking of phytoplankton in the sea. *Oceanogr. Mar. Biol. Ann. Rev.*, *8*, 353-414.
88. Somayajulu, B.L.K., Bhushan, R., Sarkar, A., Burr, G.S. and Jull, A.J.T., 1999. Sediment deposition rates on the continental margins of the eastern Arabian Sea using 210Pb, 137Cs and 14C. Science of the total environment, 237, 429-439. https://doi.org/10.1016/S0048-9697(99)00155-2
89. Subrahmanyan, R., 1959. Studies on the phytoplankton of the west coast of India. *Proceedings: Plant Sciences*, *50*(3), 113-187.https://doi.org/10.1007/BF03051925
90. Subrahmanyan, R., Sarma, A.H., 1965. Studies on the phytoplankton of the west coast of India. Part IV. Magnitude of the standing crop for 1955-1962, with observations on nanoplankton and its significance to fisheries. *Journal of the Marine Biological Association of India*, *7*(2), 406-419.
91. Sudheesh, V., Gupta, G.V.M., Reddy, Y., Bepari, K.F., Chari, N.V.H.K., Sherin, C.K., Shaju, S.S., Ramu, C.V. and Vijayan, A.K., 2022. Oxygen minimum zone along the eastern Arabian Sea: intra-annual variation and dynamics based on ship-borne studies. *Progress in Oceanography*, 201, p.102742. https://doi.org/10.1016/j.pocean.2022.102742
92. Suthhof, A., Jennerjahn, T.C., Schäfer, P.,Ittekkot, V., 2000. Nature of organic matter in surface sediments from the Pakistan continental margin and the deep Arabian Sea: amino acids. *Deep Sea Research Part II: Topical Studies in Oceanography*, *47*(1-2), 329-351.https://doi.org/10.1016/S0967-0645(99)00109-5
93. Taucher, J., Bach, L.T., Prowe, A.F., Boxhammer, T., Kvale, K., Riebesell, U., 2022. Enhanced silica export in a future ocean triggers global diatom decline. *Nature*, *605*(7911), 696-700.https://doi.org/10.1038/s41586-022-04687-0
94. TerBraak, C.J., Smilauer, P., 2002. *CANOCO reference manual and CanoDraw for Windows user's guide: software for canonical community ordination (version 4.5)*. www. canoco. com.
95. Thomas L.C., Padmakumar K.B., Smitha B.R., Devi C.A, Nandan S.B., Sanjeevan V.N., 2013. Spatio-temporal variation of microphytoplankton in the upwelling system of the south-eastern Arabian Sea during the summer monsoon of 2009. *Oceanologia* 55(1):185. https://doi.org/10.5697/oc.55-1.185

96. Tomas, C.R. ed., 1997. Identifying marine phytoplankton. Elsevier.
97. Tréguer, P.J., De La Rocha, C.L., 2013. The world ocean silica cycle. *Annual review of marine science*, *5*, 477-501.https://doi.org/10.1146/annurev-marine-121211-172346
98. Tuchman, M.L., Theriot, E., Stoermer, E.F., 1984. Effects of low level salinity concentrations on the growth of Cyclotella meneghinianaKütz. (Bacillariophyta). *ArchivfürProtistenkunde*, *128*(4), 319-326.https://doi.org/10.1016/S0003-9365(84)80003-2
99. Vijayan, A.K., Reddy, B.B., Sudheesh, V., Marathe, P.H., Nampoothiri, V.N., Harikrishnachari, N.V., Kavya, P., Gupta, G.V.M., Ramanamurthy, M.V., 2021. Phytoplankton community structure in a contrasting physico-chemical regime along the eastern Arabian Sea during the winter monsoon. *Journal of Marine Systems*, *215*, 103501.https://doi.org/10.1016/j.jmarsys.2020.103501
100. Volk, T., Hoffert, M.I., 1985. Ocean carbon pumps: Analysis of relative strengths and efficiencies in ocean-driven atmospheric CO_2 changes. *The carbon cycle and atmospheric CO2: Natural variations Archean to present*, *32*, 99-110.https://doi.org/10.1029/GM032p0099
101. Waite, A., Fisher, A., Thompson, P.A. and Harrison, P.J., 1997. Sinking rate versus cell volume relationships illuminate sinking rate control mechanisms in marine diatoms. *Marine Ecology Progress Series*, *157*, 97-108. https://doi.org/10.3354/meps157097
102. Zhang, L., Wang, R., Chen, M., Liu, J., Zeng, L., Xiang, R., & Zhang, Q., 2015. Biogenic silica in surface sediments of the South China Sea: Controlling factors and paleoenvironmental implications. *Deep Sea Research Part II: Topical Studies in Oceanography*, *122*, 142-152. https://doi.org/10.1016/j.dsr2.2015.11.008
103. Zúñiga, D., Sanchez-Vidal, A., Flexas, M.D.M., Carroll, D., Rufino, M.M., Spreen, G., Calafat, A. and Abrantes, F., 2021. Sinking diatom assemblages as a key driver for deep carbon and silicon export in the Scotia Sea (Southern Ocean). Frontiers in Earth Science, 9, p.579198. https://doi.org/10.3389/feart.2021.579198

Legends to figures

Figure 1 The upper two panels depict the oceanographic settings in the Arabian Sea during (A) summer and (B) winter monsoons. In panel A, the marked cyan-blue areas show the coastal upwelling caused by summer winds (June-September). At the same time, a low-level jet (Findlater jet; shown with yellow arrow) blows perpendicular to the Oman-Somali coast (along 16-18 °N) causing open-ocean upwelling to the north of the jet axis. The black dashed line demarks the outer boundary of the permanent Oxygen Minimum Zone (OMZ) (Redrawn from Naqvi 1991). The "red dots" represent the sampling locations of the current study, and the locations for our previous study (Pandey et al. 2023) are shown in "yellow dots". The region marked as 'FFF' corresponds to Fifty Fathom Flat near Mumbai region. In panel B the white dashed box shows the area that gets impacted by winter convective mixing (December-February). The Western Indian Coastal Current (WICC) is shown in the red arrow that flows poleward during the winter monsoon and reverses with the onset of the summer. Panel C represents the bubble map showing the absolute abundance (AA) of diatom frustules (valves g^{-1} dry sediment), and panel (D) represents the Shannon-Wiener (H') diversity index of frustules retrieved from the surface sediments of the western Indian continental shelf (Eastern Arabian Sea) along the 200 m isobaths (n =2±SD).

Figure 2 The map shows the occurrences of frustules in the sampling locations. The bubble size corresponds to the abundance of diatom frustules. The "donut chart" on the right represents the relative abundance (RA %) of diatoms in surface sediments from the western Indian continental shelf ("others" denotes individual taxa contributions <3%). The boundary line of the OMZ (Redrawn from Naqvi 1991) is displayed here in black dashed line suggesting its expansion till ~15°N and absent below that.

Figure 3 Images of the major diatoms (light microscopy) from the surface sediments of the western Indian continental shelf. A–C. *Thalassiosira* spp. D–E *Coscinodiscus* spp. F–G *Nitzschia* spp. (scale bar 10 µm).

Figure 4 Scanning Electron Microscopy (SEM) images of selected diatoms from surface sediments of western Indian continental shelf A. *Thalassiosira* sp. B. *Coscinodiscus* sp. C. *Nitzschia interruptestriata* D. *Cyclotella* sp. E. *Thalassionema fraunfeldii* F. *Thalassionema nitzschiodes* G. *Pseudo-nitzschia* sp. H. *Fragilariopsis doliolus* I. *Fragilaria* sp. (scale bar under the image).

Figure 5 Images of minor diatoms (light microscopy) from the surface sediments of the western Indian continental shelf. A *Cyclotella* sp. B. *Pseudo-nitzschia* sp. C-D. *Fragilariopsis* sp. E. *Navicula* sp. F-G. *Chaetoceros* resting spore H-I. *Cerataulina* resting spore J. *Diploneis* sp. K. *Rhizosolenia* sp. L. *Surirella* sp. M. *Hemidiscus* sp. N. *Actinoptychus* sp. O. *Triceratium* sp. P. *Paralia* sp. Q. *Asteromphalus* sp. R. *Bacteriastrum* sp. S. *Odontella* sp. (Scale bar 10 µm).

Figure 6 (A) total inorganic carbon (TIC) (%); (B) total organic carbon (TOC), (%)and (C) (TN) total nitrogen (%)in surface sediments of the western Indian continental shelf (Eastern Arabian Sea) along the 200 m isobaths (n =2±SD).

Figure 7 Redundancy analysis (RDA) biplot that represents the interrelationship between sedimentary geochemical parameters (red arrows) and biological constituents (violet arrows). The first two axes of the RDA

analysis revealed 95.8% of the total variance between abiotic and biotic components. Axis 1 and axis 2 explained 83.5% and 12.3% of the variance, respectively.

Supplementary Figure 1 Frustule abundance of centric and pennate diatoms (A); diatom frustules from three different size classes; <30 µm, 30-60 µm, and >60 µm (B); the frustule abundance of *Thalassiosira* (C); and *Coscinodiscus* (D) from three different size categories (<30 µm, 30-60 µm, and >60 µm) from the surface sediments of the western Indian continental shelf (Eastern Arabian Sea). Moving from left to right indicates the north-to-south direction along the 200 m isobaths (n =2±SD). The contribution of major and minor diatom genera is shown in the donut chart with individual contribution from diatoms (>2 % relative abundance is shown; others include diatoms with relative percentage <1%) (E) and the correlation between total organic carbon (TOC %) and total nitrogen (TN %) (F).

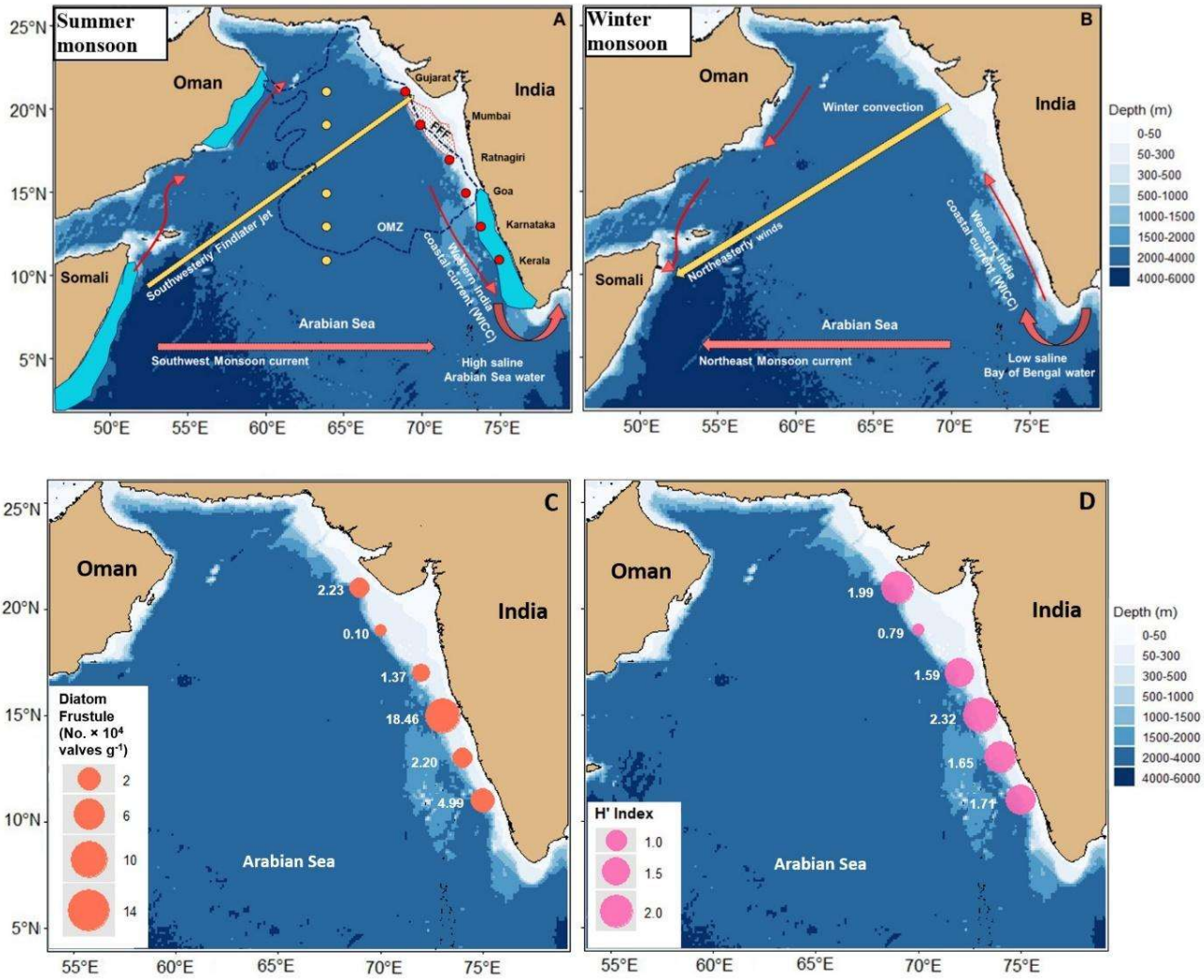

902

903

904 **Figure 1** The upper two panels depict the oceanographic settings in the Arabian Sea during (A) summer and (B)
905 winter monsoons. In panel A, the marked cyan-blue areas show the coastal upwelling caused by summer winds
906 (June-September). At the same time, a low-level jet (Findlater jet; shown with yellow arrow) blows perpendicular
907 to the Oman-Somali coast (along 16-18 °N) causing open-ocean upwelling to the north of the jet axis. The black
908 dashed line demarks the outer boundary of the permanent Oxygen Minimum Zone (OMZ) (Redrawn from Naqvi
909 1991). The "red dots" represent the sampling locations of the current study, and the locations for our previous
910 study (Pandey et al. 2023) are shown in "yellow dots". The region marked as 'FFF' corresponds to Fifty Fathom
911 Flat near Mumbai region. In panel B the white dashed box shows the area that gets impacted by winter convective
912 mixing (December-February). The Western Indian Coastal Current (WICC) is shown in the red arrow that flows
913 poleward during the winter monsoon and reverses with the onset of the summer. Panel C represents the bubble
914 map showing the absolute abundance (AA) of diatom frustules (valves g^{-1} dry sediment), and panel (D) represents
915 the Shannon-Wiener (H') diversity index of frustules retrieved from the surface sediments of the western Indian
916 continental shelf (Eastern Arabian Sea) along the 200 m isobaths (n =2±SD).

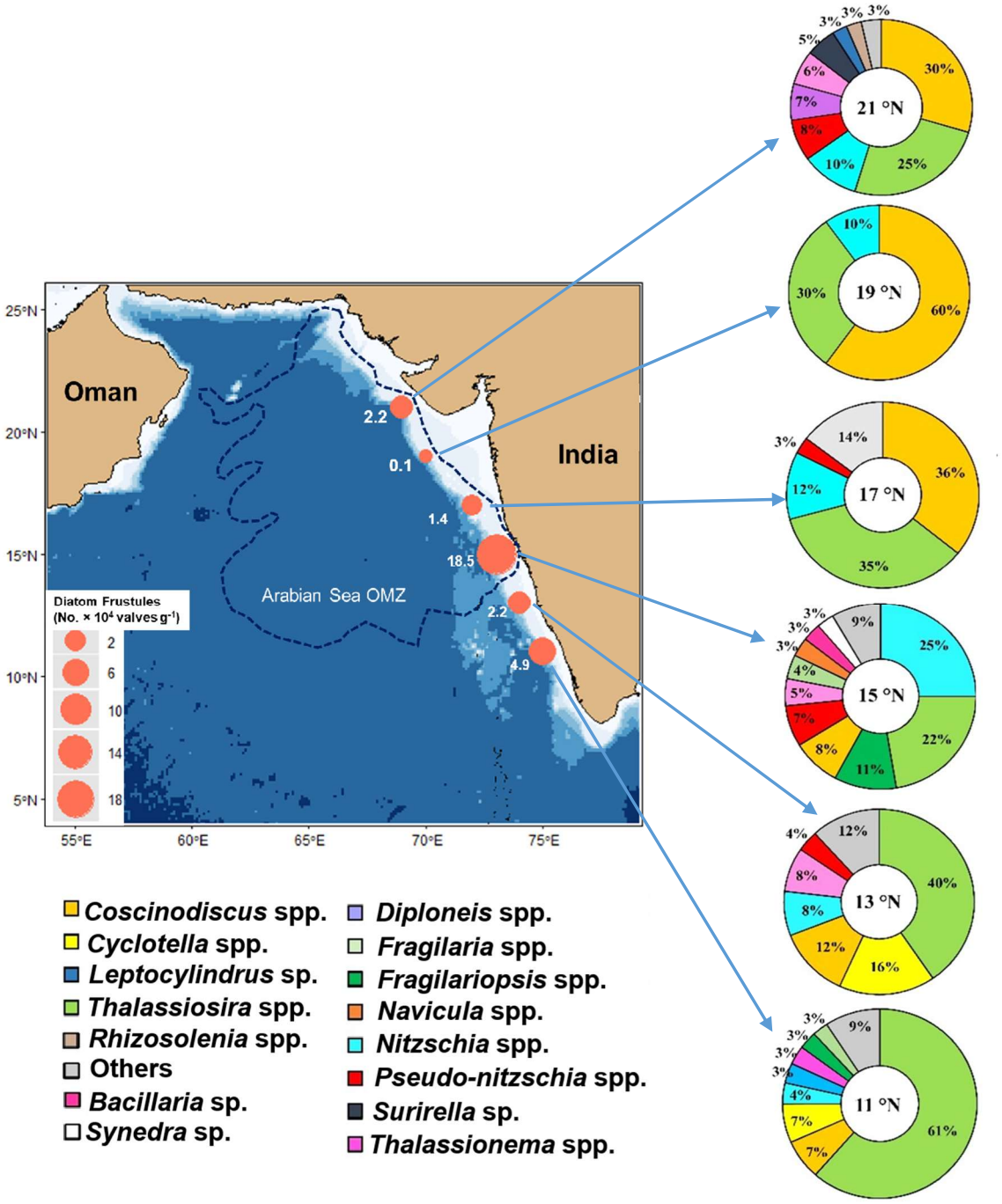

Figure 2 The map shows the occurrences of frustules in the sampling locations. The bubble size corresponds to the abundance of diatom frustules. The "donut chart" on the right represents the relative abundance (RA %) of diatoms in surface sediments from the western Indian continental shelf ("others" denotes individual taxa contributions <3%). The boundary line of the OMZ (Redrawn from Naqvi 1991) is displayed here in the black dashed line suggesting its expansion till ~15°N and absent below that.

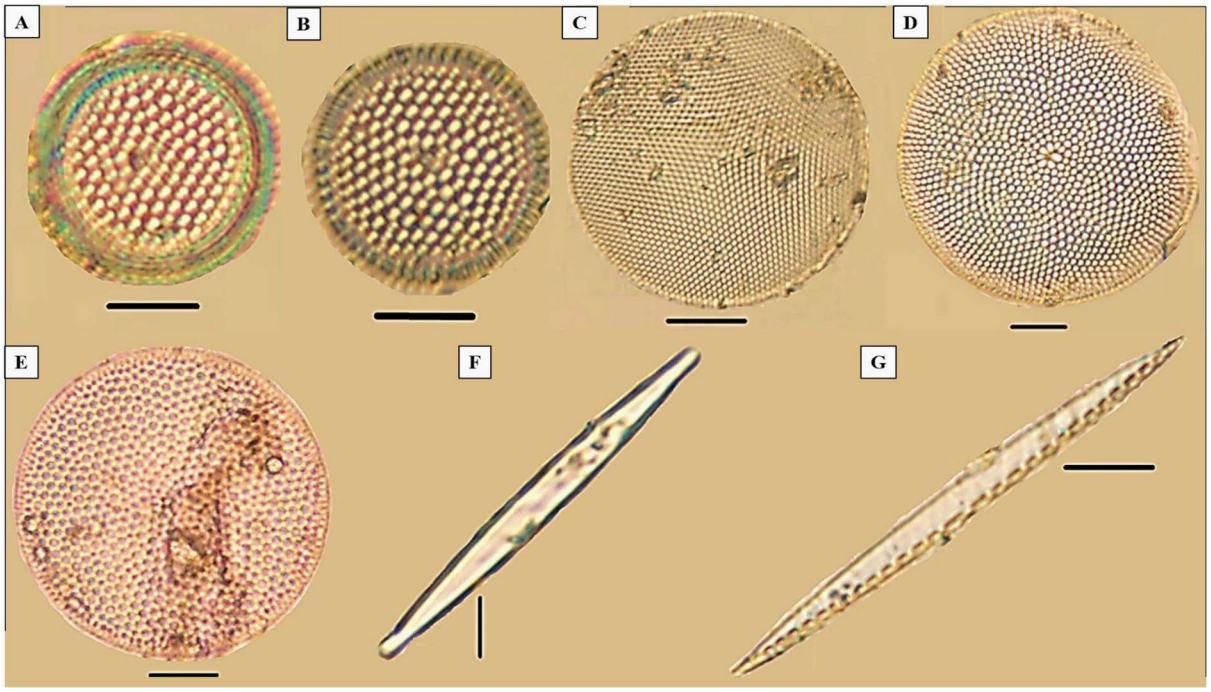

Figure 3 The images of major diatoms (light microscopy) from the surface sediments of the western Indian continental shelf. A–C. *Thalassiosira* spp. D–E *Coscinodiscus* spp. F–G *Nitzschia* spp. (scale bar 10 µm).

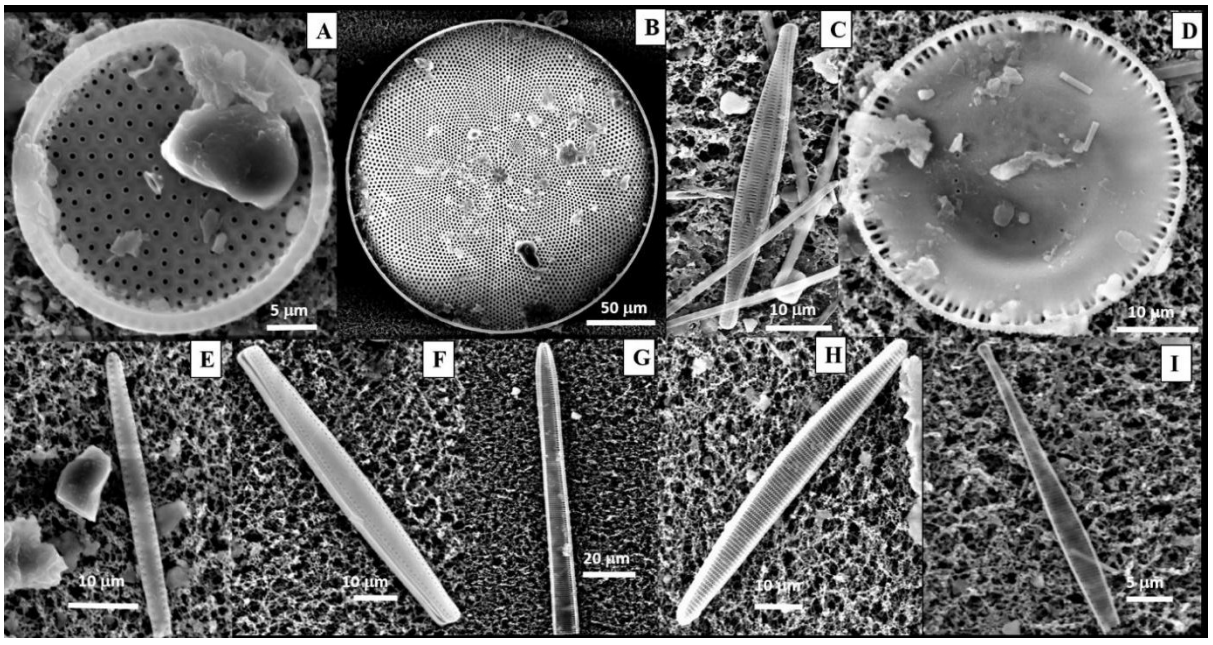

Figure 4 Scanning Electron Microscopy (SEM) images of few diatoms from surface sediments of western Indian continental shelf A. *Thalassiosira* sp. B. *Coscinodiscus* sp. C. *Nitzschia interruptestriata* D. *Cyclotella* sp. E. *Thalassionema fraunfeldii* F. *Thalassionema nitzschiodes* G. *Pseudo-nitzschia* sp. H. *Fragilariopsis doliolus* I. *Fragilaria* sp. (scale bar under the image).

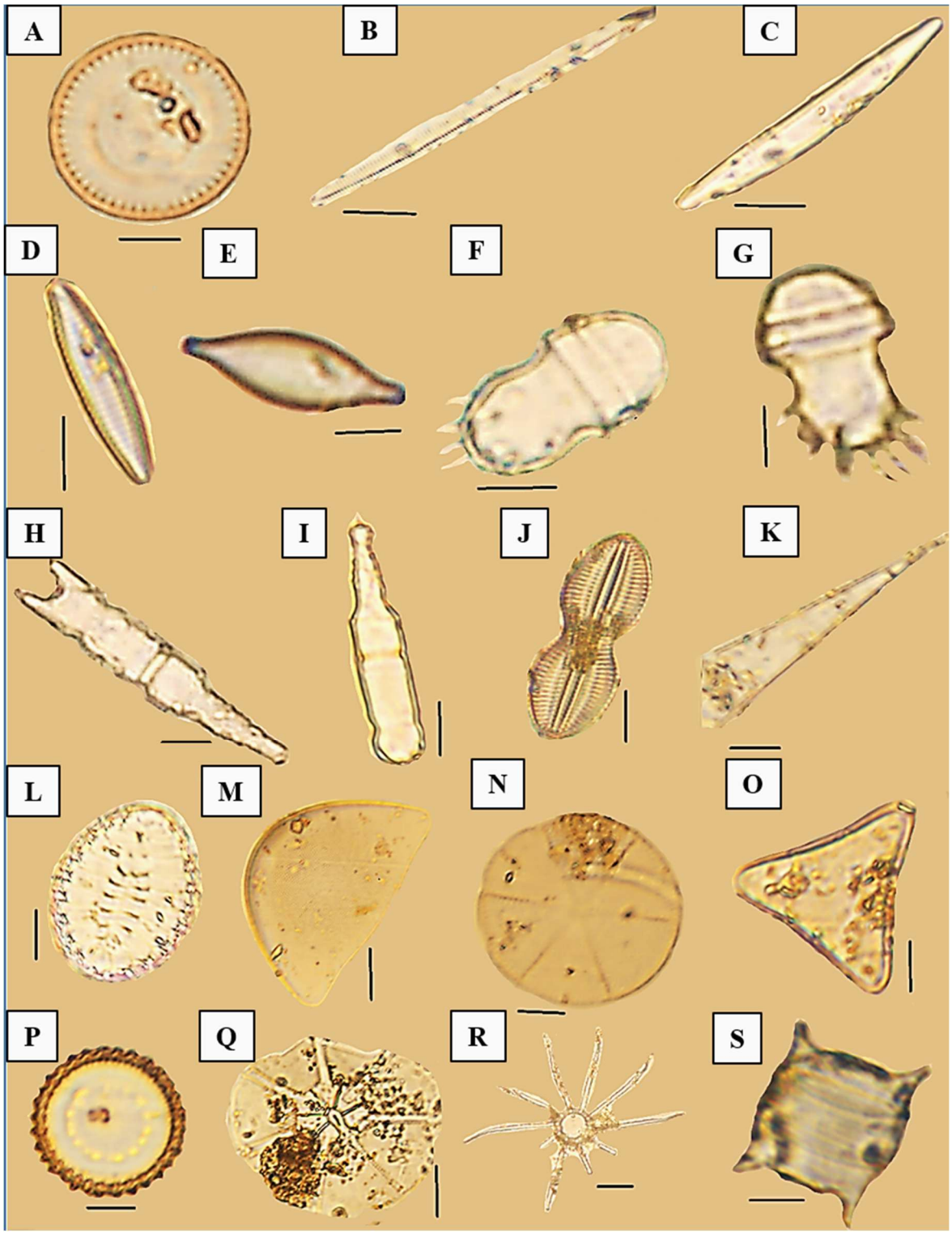

Figure 5 The images of minor diatoms (light microscopy) from the surface sediments of the western Indian continental shelf. A *Cyclotella* sp. B. *Pseudo-nitzschia* sp. C-D. *Fragilariopsis* sp. E. *Navicula* sp. F-G. *Chaetoceros* resting spore H-I. *Cerataulina* resting spore J. *Diploneis* sp. K. *Rhizosolenia* sp. L. *Surirella* sp. M. *Hemidiscus* sp. N. *Actinoptychus* sp. O. *Triceratium* sp. P. *Paralia* sp. Q. *Asteromphalus* sp. R. *Bacteriastrum* sp. S. *Odontella* sp. (Scale bar 10 µm).

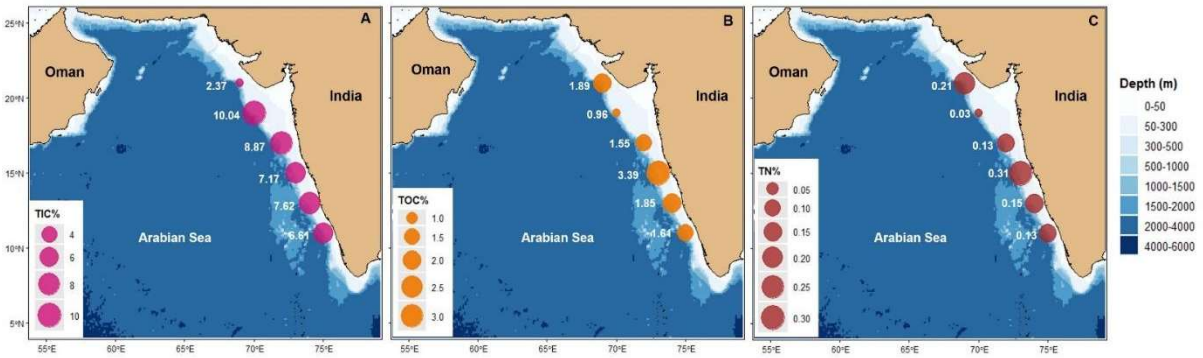

Figure 6 The contents of (A) total inorganic carbon (%) (TIC); (B) total organic carbon (%) (TOC), and (C) total nitrogen (%) (TN) from the surface sediments of the western Indian continental shelf (Eastern Arabian Sea) along the 200 m isobaths (n =2±SD).

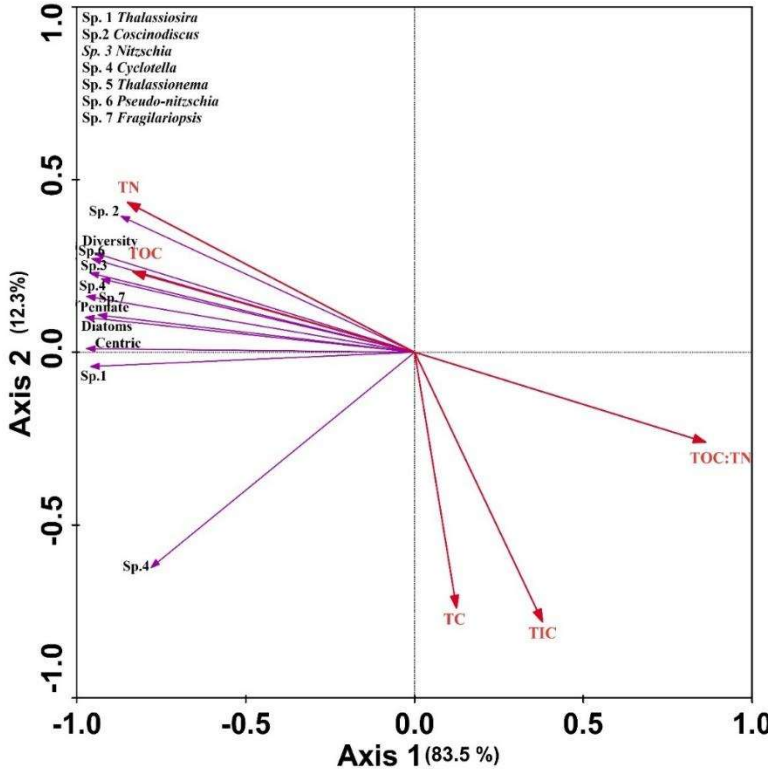

Figure 7 The redundancy analysis (RDA) biplot represents the interrelationship between sedimentary geochemical parameters (red arrows) and biological constituents (violet arrows). The first two axes of the RDA analysis revealed 95.8% of the total variance between abiotic and biotic components. Axis 1 and axis 2 explained 83.5% and 12.3% of the variance, respectively.

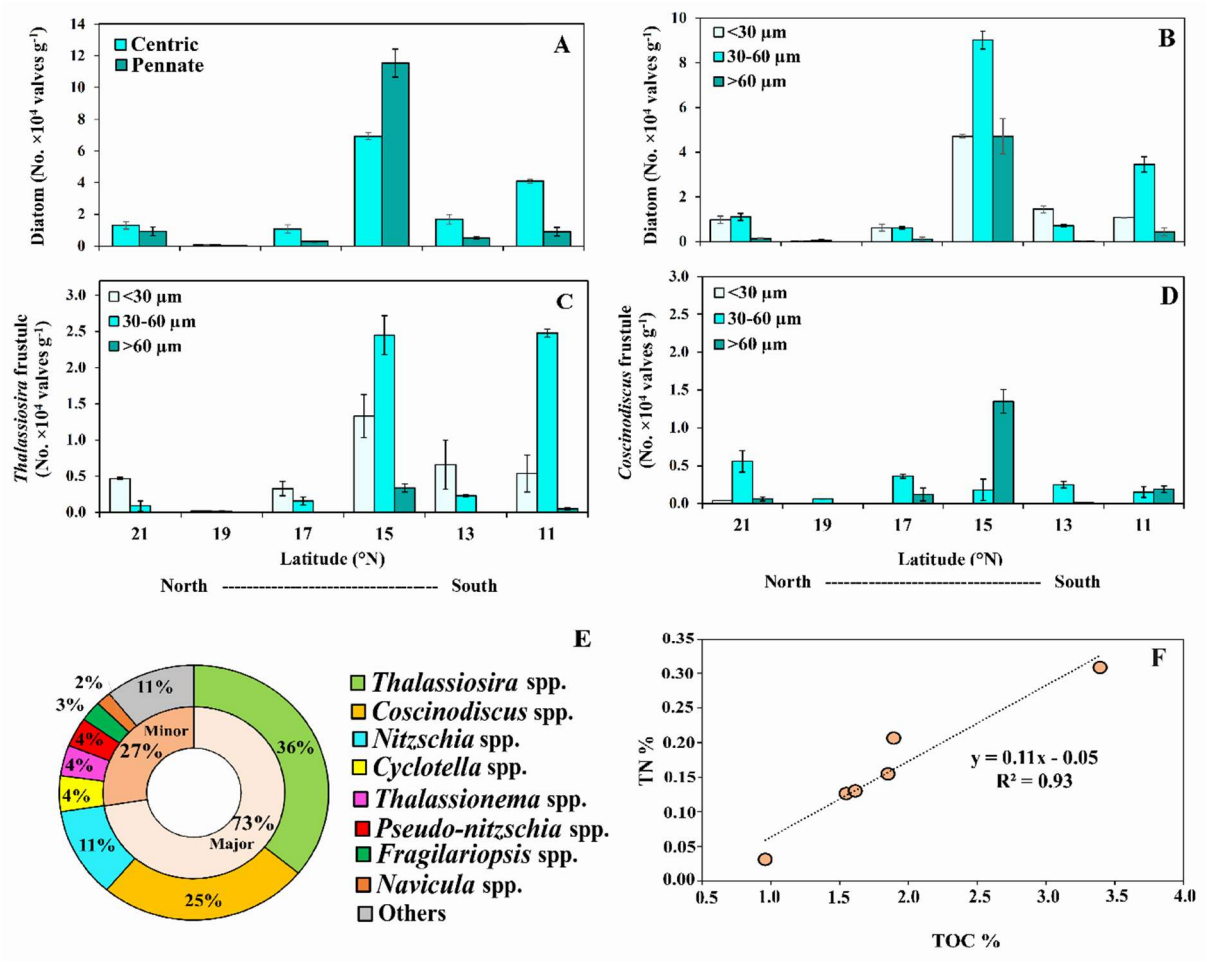

Supplementary Figure 1 Frustule abundance of centric and pennate diatoms (A); diatom frustules from three different size classes; <30 µm, 30-60 µm, and >60 µm (B); the frustule abundance of *Thalassiosira* (C); and *Coscinodiscus* (D) from three different size categories (<30 µm, 30-60 µm, and >60 µm) from the surface sediments of the western Indian continental shelf (Eastern Arabian Sea). Moving from left to right indicates the north-to-south direction along the 200 m isobaths (n =2±SD). The contribution of major and minor diatom genera is shown in the donut chart with individual contribution from diatoms (>2 % relative abundance is shown; others include diatoms with relative percentage <1%) (E) and the correlation between total organic carbon (TOC %) and total nitrogen (TN %) (F).

Table 1. Details of dry bulk density (DBD), mass accumulation rate (MAR), diatom valve concentration (DVC), and diatom valve flux (derived using $210Pb_{excess}$) collected from 11, 13, 15° N at 200m isobaths of western Indian continental shelf (eastern Arabian Sea). The MAR for 21°N was calculated using the sedimentation rate from Somayajulu et al., 1999.

Latitude (°N)	Dry bulk density (DBD; g cm^{-3})	Sediment accumulation rate (SAR; g cm^{-3})	Mass accumulation rate (MAR; g cm^{-2} yr^{-1})	Diatom valve concentration (DVC; valve × 10^4 g-1)	Diatom valve flux (valves × 10^3 cm^{-2} yr^{-1})
21	0.44	0.22	0.096	2.23	2.14
19	-	-	-	0.10	-
17	0.64	0.016	0.011±0.003	1.37	0.15
15	0.30	0.05	0.018± 0.001	18.46	3.39
13	0.65	0.13	0.093± 0.010	2.20	2.05
11	0.65	0.27	0.203± 0.058	4.99	10.14

Table 2. Characteristics of surface sediments from the Western Indian Continental Shelf (eastern Arabian Sea) showing total inorganic carbon = TIC, calcium carbonate (CaCO3), total organic carbon = TOC, total nitrogen =TN, (values ± SD).

Latitude (°N)	TIC (%)	$CaCO_3$ (%)	TOC (%)	TOC (mg g^{-1})	TN (%)	Diatom Frustules (No. $\times 10^4$ valves g^{-1})	Shannon-Wiener index (H')
21	2.37±0.08	19.74±0.67	1.89±0.09	18.9	0.21±0.001	2.23±0.04	1.99±0.12
19	10.04±0.04	83.59±0.35	0.96±0.03	9.6	0.03±0.005	0.10±0.03	0.79±0.32
17	8.87±0.07	73.89±0.61	1.55±0.06	15.5	0.13±0.001	1.37±0.30	1.59±0.07
15	7.17±0.13	59.76±1.08	3.39±0.12	33.9	0.31±0.006	18.46±1.10	2.32±0.07
13	7.62±0.01	63.50±0.11	1.85±0.02	18.5	0.15±0.006	2.20±0.23	1.91±0.17
11	6.61±0.03	55.03±0.29	1.61±0.04	16.1	0.13±0.002	4.99±0.16	1.65±0.20
Average±SD	7.11±2.63	59.25±0.52	1.88±0.81	18.8	0.16±0.09	4.89±6.84	1.71±0.52

Table 3. The absolute abundance (AA) of individual diatom frustules is expressed as valves g^{-1} dry sediment and relative abundance (RA) (%) calculated from the microscopic analysis of the surface sediments from different locations of the Eastern Arabian Sea (n = 2; ±SD). The abbreviations 'c' and 'p' correspond to centric and pennate diatoms, respectively.

Type	Diatom frustules	21° N		19° N		17° N		15° N		13° N		11° N			
		AA	RA	AA	RA	AA	RA	AA	RA	AA	RA	AA	RA	Average AA	Average RA
p	***Achnanthes* spp.**	0	0.0	0	0.0	200±283	1.5	100±141	0.1	500±141	2.3	0	0.0	133±197	0.6
c	***Actinoptychus* spp.**	0	0.0	0	0.0	300±141	2.2	900±424	0.5	100±141	0.5	200±0	0.4	250±339	0.6
p	***Amphiprora* sp.**	0	0.0	0	0.0	0	0.0	0	0.0	0	0.0	200±283	0.4	33±82	0.1
p	***Asterionellopsis* sp.**	0	0.0	0	0	0	0.0	100±141	0.1	0	0.0	0	0.0	17±41	0.0
c	***Asteromphalus* spp.**	0	0.0	0	0.0	100±141	0.7	500±141	0.3	0	0.0	0	0.0	100±200	0.2
p	***Bacillaria* sp.**	0	0.0	0	0.0	0	0.0	5800±1414	3.1	0	0.0	100±141	0.2	983±2360	0.6
c	***Bacteriastrum* sp.**	0	0.0	0	0.0	0	0.0	400±283	0.2	0	0.0	100±141	0.2	83±160	0.1
c	***Cerataulina* resting spore**	0	0.0	0	0.0	0	0.0	300±424	0.2	400±0	1.8	400±0	0.8	183±204	0.5

c	***Chaetoceros* resting spore**	0	0.0	0	0.0	0	0.0	900±141	0.5	500±141	2.3	100±141	0.2	250±373	0.5
p	***Cocconeis* sp.**	100±141	0.4	0	0.0	0	0.0	500±424	0.3	0	0.0	0	0.0	100±200	0.1
c	***Coscinodiscus* spp.**	6600±1131	29.6	600±0	60.0	4800±566	35.0	15300±141	8.3	2700±424	12.3	3400±283	6.8	5567±5176	25.3
c	***Cyclotella* spp.**	0	0.0	0	0.0	300±141	2.2	3900±141	2.1	3600±849	16.4	3300±1273	6.6	1850±1930	4.5
p	***Cymbella* sp.**	0	0.0	0	0.0	0	0.0	200±0	0.1	0	0.0	0	0.0	33±82	0.0
p	***Diploneis* spp.**	1500±707	6.7	0	0.0	0	0.0	500±141	0.3	0	0.0	400±283	0.8	400±583	1.3
p	***Fragilaria* spp.**	0	0.0	0	0.0	0	0.0	7700±141	4.2	0	0.0	1300±707	2.6	1500±3082	1.1
p	***Fragilariopsis* spp.**	200±0	0.9	0	0.0	100±141	0.7	19500±1838	10.6	100±141	0.5	1500±424	3.0	3567±7826	2.6
p	***Gomphonema* sp.**	0	0.0	0	0.0	0	0.0	600±283	0.3	0	0.0	300±424	0.6	150±251	0.2
c	***Hemidiscus* spp.**	100±141	0.4	0	0.0	200±0	1.5	2200±283	1.2	100±141	0.5	200±0	0.4	467±852	0.7

c	***Leptocylindrus* sp.**	0	0.0	0	0.0	0	0.0	400±566	0.2	0	0.0	1700±424	3.4	350±680	0.6
p	***Licmophora* sp.**	0	0.0	0	0.0	0	0.0	200±283	0.1	0	0.0	0	0.0	33±82	0.0
p	***Lyrella* sp.**	100±141	0.4	0	0.0	0	0.0	0	0.0	0	0.0	100±141	0.2	33±52	0.1
p	***Navicula* spp.**	600±283	2.7	0	0.0	300±141	2.2	6100±1556	3.3	300±141	1.4	600±283	1.2	1317±2354	1.8
p	***Nitzschia* spp.**	2300±141	10.3	100±141	10.0	1600±283	11.7	46200±2546	25.0	1700±141	7.7	1800±283	3.6	8950±18264	11.4
c	***Odontella* sp.**	0	0.0	0	0.0	0	0.0	100±141	0.1	0	0.0	0	0.0	17±41	0.0
c	***Paralia* sp.**	0	0.0	0	0.0	0	0.0	0	0.0	0	0.0	500±141	1.0	83±	0.2
p	***Pinnularia* sp.**	0	0.0	0	0.0	0	0.0	0	0.0	0	0.0	100±141	0.2	17±204	0.0
p	***Pleurosigma* spp.**	0	0.0	0	0.0	100±141	0.7	100±141	0.1	0	0.0	200±0	0.4	67±41	0.2
p	***Pseudo-nitzschia* spp.**	1700±141	7.6	0	0.0	400±566	2.9	13200±1414	7.2	800±283	3.6	500±141	1.0	2767±5143	3.7

c	***Rhizosolenia* spp.**	600±283	2.7	0	0.0	200±283	1.5	2300±424	1.2	400±0	1.8	100±141	0.2	600±860	1.2
p	***Surirella* sp.**	1200±283	5.4	0	0.0	0	0.0	300±141	0.2	0	0.0	200±283	0.4	283±467	1.0
p	***Synedra* sp.**	0	0.0	0	0.0	0	0.0	5400±1131	2.9	0	0.0	0	0.0	900±2205	0.5
p	***Thalassionema* spp.**	1400±1131	6.3	0	0.0	200±283	1.5	8700±2121	4.7	1700±141	7.7	1600±283	3.2	2267±3235	3.9
c	***Thalassiosira* spp.**	5600±566	25.1	300±141	30.0	4900±1556	35.8	41200±283	22.3	8900±3536	40.5	30700±2121	61.5	15267±16590	35.9
c	***Triceratium* spp.**	100±141	0.4	0	0.0	0	0.0	700±424	0.4	200±0	0.9	100±141	0.2	183±264	0.3
c	**Unknown Centric**	0	0.0	0	0.0	0	0.0	100±141	0.1	0	0.0	0	0.0	17±41	0.0
p	**Unknown Pennate**	200±283	0.9	0	0.0	0	0.0	200±283	0.1	0	0.0	200±0	0.4	100±110	0.2
	Total diatom frustule	22300±1471		1000±111		13700±1134		184600±10607		22000±1634		49900±5099			

1033

1034

Table 4. Absolute abundance of diatom frustules from different size classes, centric, pennate, and for two major contributing genera (*Thalassiosira* and *Coscinodiscus*) from surface sediments from the Western Indian Continental Shelf (eastern Arabian Sea) (values ± SD).

Latitude (°N)	Diatom frustules from three size classes (No. $\times 10^4$ valves g^{-1})			Centric Diatom (No. $\times 10^4$ valves g^{-1})	Pennate Diatom (No. of valves $\times 10^4$ cells g^{-1})	*Thalassiosira* frustule in sediment (No. $\times 10^4$ valves g^{-1})			*Coscinodiscus* frustule in sediment (No. $\times 10^4$ valves g^{-1})		
	<30µm	30–60 µm	>60 µm			<30µm	30–60 µm	>60 µm	<30µm	30–60 µm	>60 µm
21	0.98± 0.17	1.11± 0.16	0.14± 0.03	1.30± 0.23	0.93±0.27	0.47± 0.01	0.09± 0.07	0	0.04± 0.00	0.56± 0.14	0.06± 0.03
19	0.03± 0.01	0.07± 0.01	0	0.09± 0.01	0.01±0.01	0.02± 0	0.01± 0.01	0	0	0.06± 0	0
17	0.63± 0.16	0.62± 0.06	0.12± 0.08	1.08± 0.25	0.29±0.04	0.33± 0.10	0.16± 0.06	0	0	0.36± 0.03	0.12± 0.08
15	4.72± 0.08	9.02± 0.40	4.72± 0.79	6.92± 0.23	11.54± 0.88	1.33± 0.30	2.45± 0.27	0.34± 0.06	0	0.18± 0.14	1.35± 0.16
13	1.45± 0.16	0.72± 0.06	0.03± 0.01	1.69± 0.30	0.51±0.07	0.66± 0.34	0.23± 0.01	0	0	0.25± 0.04	0.02± 0.00
11	1.09± 0.01	3.46± 0.34	0.44± 0.17	4.08± 0.11	0.91±0.27	0.54± 0.25	2.48± 0.06	0.05± 0.01	0	0.15± 0.07	0.19± 0.04
Average±SD	1.48± 1.66	2.50± 3.41	0.91± 1.87	2.53± 2.53	2.37±4.51	0.56± 0.44	0.90± 1.21	0.07± 0.14	0.01± 0.02	0.26± 0.18	0.29± 0.52

1050 **Table 5.** The list of major diatom species from the coastal waters of the Eastern Arabian Sea was reported in
1051 earlier studies during both the southwest monsoon (SWM) and northeast monsoon (NEM). The studies reported
1052 close to our sampled stations are considered.

1053

Source	Duration	Location	Parameter studied	Major diatom species found
Chowdhury and Biswas, 2023	SWM (Aug 2017-2018)	8-21 °N at one-degree interval 200 m isobath	Phytoplankton and pigment study	*Chaetoceros* sp., *Dactyliosolen fragilissimus*, *Thalassiosira* sp., *Pseudo-nitzschia* sp., *Navicula* sp., *Coscinodiscus* sp., *Rhizosolenia* sp., *Cyclotella* sp., *Pleurosigma* sp.
Albin et al., 2022	NEM and SWM	19° N, 66.8° E; 20.4° N, 66 ° E; 21° N, 67° E	Phytoplankton community	*Chaetoceros*, *Coscinodiscus*, *Dictyocha*, *Heliotheca*, *Hemiaulus*, *Hemidiscus*, *Navicula*, *Nitzschia*, *Odontella*, *Planktionella*, *Pleurosigma*, *Pseudo-Nitzschia*, *Rhizosolenia*, *Thalassionema*, *Thalassiosira*
Sathish et al., 2022	NEM	9 to 15° N, 73 to 76° E	Phytoplankton community	*Chaetoceros*, *Bacteriastrum*, and *Leptocylindrus*
Vijayan et al., 2021	NEM	7 to 21° N, 68 to 78° E	Pigment studies	North and south coastal regions were dominated by diatoms by 96 % and 55% respectively.
Jyothibabu et al., 2021	SWM	9° N, 76° E	Phytoplankton community	*Thalassiosira*, *Thalassionema*, *Asterionellopsis, Streptotheca, Fragilariopsis, Chaetoceros. Bacteriastrum, Hemisdiscus, Coscinodiscus, Rhizosolenia, Guinardia, Stephnopyxis*
Karnan et al., 2020	SWM	9° 55' N, 76-76.25° E	Phytoplankton community	*Fragilaria*, *Thalassiosira*, *Thalassionema*, *Skeletonema*
Ahmed et al., 2016	SWM	8 to 17° N at 0.5° interval (water depth range: 600-800m)	Pigment studies and phytoplankton community	South of 12 °N dominated by large diatoms (*Chaetoceros coarctatum* and *Nitzschia*); north of 12 °N picoplankton and nanoplankton dominated.
Thomas et al., 2013	SWM	8 to 10° N, 75 to 77° E	Phytoplankton community	*Chaetoceros*, *Nitzschia*, *Pseudo-nitzschia*, *Amphora*, *Navicula*
Habeebrehman et al., 2008	SWM	8 to 19° N, 70 to 78° E	Phytoplankton community	*Nitzschia seriata*, *Rhizosolenia alata*, *Thalassiosira subtilis*, *Skeletonema costatum*, *Rhizosolenia setigera*
Parab et al., 2006	NEM and SWM	15.51° N, 73.16° E	Pigment and phytoplankton community	*Chaetoceros lorenzianus*, *Nitzschia closterium*, *Rhizosolenia imbricate*, *Thalassiosira condensate*, *Navicula acuminate*, *Thalassionema nitzschoides*, *Thalassiosira eccentrica*, *Gyrosigma littorale, Coscinodiscus centralis*
Gopinathan et al., 2001	Post SWM	7 to 20° N along the western Indian coast (water depth ranging from 40-200m)	Pigment and phytoplankton community	*Coscinodiscus*, *Thalassiosira*, *Nitzschi*a, *Eucampia*, *Planktoniella sol*, *Asterionella japonica*, *Thalassiothrix fraunfeldii*;

				Goa, Ratnagiri and Mumbai: *Biddulphia*, *Coscinodiscus*, *Nitzschia*, *Rhizosolenia*, *Thalassiosira* and *Eucampia*
Sawant and Madhupratap, 1996	SWM, NEM, and spring inter-monsoon	21° N, 67° E; 19° N, 70° E; 15° N, 70° E; 12° N, 74° E; 10° N, 75° E	Phytoplankton community	*Chaetoceros* sp., *Coscinodiscus* sp., *Rhizosolenia alata*, *R. stoltherfothi*, *Rhizosolenia* sp., *Navicula*, *Nitzschia* sp., *Thalassiosira* sp., *Thalassionema nitzschiodes*, *Cerataulina* sp.

1054

1055

1056

1057

1058

1059

1060